

A computer program for solving multi-level non-LTE radiative transfer problems in spherical geometry, in moving or static atmospheres

Graham M. Harper¹

Department of Physics (Theoretical Physics)
University of Oxford
1 Keble Road, Oxford OX1 3NP

ABSTRACT

The interpretation of spectra of the optically thick atmospheres of late-type stars requires that the details of radiative transfer be taken into account. For single main-sequence stars the solution of the radiative transfer problem can in most cases be made with the assumption of plane parallel geometry. For evolved late-type stars the assumption of spherical symmetry is more appropriate. We present modifications to an existing plane-parallel, non-LTE radiative transfer code – MULTI which include spherical symmetry in static and moving atmospheres. The code is suitable for application to stars where the wind velocities are up to several times the microturbulent velocity (*i.e.* where the Sobolev approximation is not valid) and where the flows are not necessarily monotonic. We compare the accuracy of the adopted scheme with previous independent techniques and find good agreement. A global approximate operator suitable for spherical geometry and complete redistribution is also presented.

Key words: radiative transfer - stars: atmospheres

1 INTRODUCTION

Spectra of evolved cool star atmospheres reflect the physical environment of the photosphere, chromosphere, wind and higher temperature material, if present. For a radiative transition that is optically thick in the chromosphere, the observed line profile may depend on: the photospheric structure through the photoionizing background radiation field; the chromosphere through the source of the excitation of the upper level, and the stellar wind, which can scatter the line photons (if there is sufficient opacity) thus modifying the line profile.

The solution of the radiative transfer problem for time-independent stellar atmospheres is the self-consistent solution to the statistical equilibrium and radiative transfer equations for a given atomic model. Many different techniques have been developed to find such solutions, either in detail or with some level of approximation. An excellent review of a selection of these techniques is given in ‘Methods in radiative transfer’ edited by Kalkofen (1984). Successful modelling of stellar

¹Present address: Joint Institute for Laboratory Astrophysics, University of Colorado at Boulder, Campus Box 440, Boulder, Colorado 80309-0440, USA.

spectra involves the construction of model atmospheres under certain assumptions, which can either quantitatively or qualitatively describe the observations.

The electron temperatures in cool star chromospheres have a range of $\sim 2000 - 20000$ K and lines excited by electrons characterized by these temperature can lie in the optical and ultraviolet wavebands. Consequently observations made with the *International Ultraviolet Explorer (IUE)* have greatly improved our understanding of cool star chromospheres (see Jordan & Linsky 1987). The modelling of cool star spectra has in the past been dominated by calculations that usually assume static atmospheres with plane-parallel geometry. Table 3 of Linsky (1985) gives a good indication of cool star models made to that date; notable exceptions to these classical assumptions being the spherically symmetric wind models of α Boo (K2 III) (Drake 1985) and α Ori (Hartmann & Avrett 1984). The assumptions of plane-parallel atmospheres are very good for main-sequence stars because the extent of the chromospheric layers is small compared to the stellar radius, and the opacity in the expanding wind is negligible for chromospheric lines. Modelling of the solar-limb spectrum also requires spherical geometry, although geometric transformations can be applied to plane-parallel calculations (*e.g.* Uitenbroek & Bruls 1992).

We present a description of modifications made to the existing plane-parallel radiative transfer code entitled ‘A computer program for solving multi-level non-LTE radiative transfer problems in moving or static atmospheres’ (Carlsson 1986; hereafter known as MULTI). These modifications allow the solution of both static and moving atmosphere problems in spherically symmetric geometry. The code is suitable for application to stars where the wind velocities are up to several times the microturbulent velocity (*i.e.* where the Sobolev approximation is not valid) and where the flows are not necessarily monotonic. A comparison of the results of the adopted scheme with results from other investigators shows that the adopted method is suitable for cool star atmospheres. The modified code is referred to as S-MULTI. In both of these codes the radiative transfer problem is solved for a given atomic model and prescribed atmospheric temperature structure.

In Section 2 we examine the likely geometric extent of cool star atmospheres and its effects on transfer problems; the modifications included in S-MULTI are described in Section 3. In Section 4 we compare results from the adopted scheme with results from independent investigations. Conclusions are given in Section 5.

2 CHROMOSPHERIC EXTENT OF EVOLVED STARS

One problem in modelling stellar spectra is to determine the extent of the atmospheric model required to calculate reliable atomic number densities. One condition is that the optical depths for all frequencies at the outer edge of the model should be much less than unity. Hydrogen Ly α is the most opaque transition in a weakly-ionized wind and it is convenient to consider the extent out to which the radial line centre optical depth of hydrogen Ly α is less than unity ($\tau_{Ly\alpha} < 1$). The ionization of hydrogen is the predominant source of free electrons in the warmer regions of the atmosphere and it is here that the solution of the coupled statistical equilibrium and radiative transfer equations for hydrogen determines the ionization balance. The optical depth is *formally* measured from the position of the observer but since we often wish to separate out the effects

of the Earth’s atmosphere and the interstellar medium, the optical depth is more usefully measured from the boundary between the stellar atmosphere/wind and the interstellar medium. This represents a discontinuity in thermodynamic properties and velocity fields and represents a convenient delimitation since the interstellar absorption can then be modelled separately. The effects of the interstellar radiation field could be included in calculations via diffuse illumination at the outer boundary condition (*e.g.* Rogers & Glassgold 1991). The interstellar medium will not, in general, be static in the reference frame of the star and the outer atmosphere may be markedly non-spherical. The influence of these outer atmospheric regions on the inner regions of interest should not be significant compared to other uncertainties, such as some sources of opacity *in the wind* which are not included in typical calculations.

The complete Earth-Star radiative transfer calculation is not currently feasible.

2.1 Evolved coronal stars

For stars with transition region plasma (and by implication coronae), the radial extent where $\tau_{Ly\alpha} = 1$ is in, or near, the transition region where the chromospheric coolants ionize and the electron temperature increases rapidly. In evolved stars, such as giants and supergiants, the lower surface gravity leads to an increase in the characteristic scale height H . The ratio of the chromospheric extent to the stellar radius is, however, a better indicator of the geometry of the problem. In the lower chromosphere the wind velocity gradients are expected to be small and the pressure scale height is determined by thermal gas pressure, P_g , and wave pressures, P_w , so we can write

$$\frac{H}{R_*} \propto \frac{R_* T_e (1 + P_w/P_g)}{M_*}. \quad (1)$$

To evaluate this expression we need to know the ratio of wave to gas pressures but little is known about the mechanisms that drive cool star winds or the wave pressure. Observations of optically thin emission lines in cool star provide upper limits to this ratio, which is less than or of the order of unity. In the quiet solar atmosphere model of Vernazza, Avrett & Loeser (1981), the ratio of the total extent of the mean chromosphere to the solar radius is $\sim 3 \times 10^{-3}$. If we assume that the chromospheric extent consists of approximately the same number of scale heights (~ 20 at 5000 K) as for other stars, then for a coronal G bright giant (*e.g.* β Dra G2 II; $R_* \sim 70R_\odot$, $M_* \sim 7M_\odot$) and coronal G supergiant (α Aqr G2 Ib; $R_* \sim 100R_\odot$, $M_* \sim 5M_\odot$) the ratio becomes 0.03 and 0.07 respectively.

The winds from coronal evolved stars may have significant opacity and require a more extended atmospheric model. For example, the ‘hybrid’ giants show the presence of a cool wind in blueshifted absorption features in the Mg II h and k resonance line emission cores, as well as coronal emission (Hartmann, Dupree & Raymond 1980, 1981). Semi-empirical models of the chromospheres and transition regions of the hybrid bright giants have similar ratios of atmospheric extension as the estimates for coronal stars above (Harper 1992) but to model the wind features would require a more extended atmospheric model.

2.2 Evolved non-coronal stars

For cool stars that show no evidence of transition region material, the neutral hydrogen column densities (and hence the chromospheric extent) will be significantly larger than for coronal stars. The extent of a cool wind atmosphere can be estimated as follows for a time-independent, spherically symmetric wind. The conservation of mass leads to the following expression for the mass-loss rate:

$$\dot{M} = 4\pi\mu m_H R^2 N_{tot}(R)V(R) \quad (2)$$

where μm_H is the mean atomic mass per particle and $\mu \leq 1.27$ for a partially ionized gas, N_{tot} is the particle density, R is the radial distance and V is the velocity, which can be assumed to be equal to the terminal velocity V_∞ in the outer layers of the atmosphere. In this case the density profile is given by

$$N_H(R) = N_H(R_0) \left(\frac{R_0}{R}\right)^2 \quad (3)$$

where $N_H(R_0)$ is the hydrogen density at a reference radius R_0 . Because the ground state of hydrogen dominates the total population $N_{H,n=1} \simeq N_H$ when the wind is weakly ionized and the density of molecular hydrogen is negligible, the optical depth at line centre in Ly α is

$$\tau_{Ly\alpha} \simeq \sigma_0 \int_{R_{ISM}}^R N_H(R) dR \quad (4)$$

where σ_0 is the line centre cross-section, and for a Doppler broadened Voigt profile, σ_0 is given by

$$\sigma_0 \simeq \frac{\lambda_0^3}{V_{Dopp}\sqrt{\pi}} \frac{g_{n=2}}{g_{n=1}} \frac{A_{21}}{8\pi} \quad (5)$$

where $\lambda_0 = 1215.67\text{\AA}$, A_{21} is the Einstein spontaneous decay rate, the g s are the statistical weights of the upper and lower levels and V_{Dopp} is the Doppler broadening parameter for the normalized line profile $\phi(\Delta V)$, where in the Doppler core

$$\phi(\Delta V) \simeq \frac{1}{V_{Dopp}\sqrt{\pi}} e^{-(\Delta V/V_{Dopp})^2}. \quad (6)$$

R_{ISM} is the radial extent out to which the wind density profile is given by equation (3) *i.e.* where the wind pressure becomes greater than or comparable to that of the interstellar medium (ISM), P_{ISM} . For illustration, if we neglect the gas pressure in the wind (*i.e.* $V_\infty > C_s$, where C_s is the sound speed in the wind) and assume that the wind density (ρ_W), is less than that in the ISM (ρ_{ISM}), then the conservation of momentum gives

$$\rho_W V_\infty^2 \left(1 - \frac{\rho_W}{\rho_{ISM}}\right) \simeq \rho_W V_\infty^2 \simeq P_{ISM}.$$

Using equation (2) we find

$$R_{ISM} \simeq \sqrt{\frac{\dot{M}}{4\pi} \frac{V_\infty}{P_{ISM}}}. \quad (7)$$

We adopt an interstellar magnetic field, B , of $\sim 5 \times 10^{-6}$ Gauss *e.g.* from the observed relationship between the interstellar B and N_H (Troland & Heiles 1986) and typical interstellar densities near the Sun (Paresce 1984), which are applicable to the nearby bright evolved stars that can be studied spectroscopically in the ultraviolet. The magnetic pressure combined with similar magnitude contributions from cosmic rays, gas and turbulent pressures gives a total pressure of $P_{ISM} \sim 10^{-12}$ dynes cm^{-2} .

Assuming that the wind is mostly neutral and that helium has an abundance relative to hydrogen of 0.1, then $N_{tot} \simeq 1.1N_H$. Equation (3) then allows us to write the optical depth at line centre as

$$\tau_{Ly\alpha} \simeq \frac{\sigma_0 \dot{M}}{4.4\pi \mu m_H V_\infty} \int_{R_{ISM}}^R \frac{1}{R^2} dR. \quad (8)$$

Setting $\tau_{Ly\alpha} = 1$, and defining $R_W \equiv \frac{\sigma_0 \dot{M}}{4.4\pi \mu m_H V_\infty}$, where R_W would be the radial extent of the atmosphere if the wind extended to infinity with the density profile given above, then we find

$$R_{\tau=1} \simeq \frac{R_W R_{ISM}}{R_{ISM} + R_W}. \quad (9)$$

We adopt the stellar parameters of ζ Aur (K4 Ib) given in Baade (1990, 1992) to evaluate these terms, *i.e.* a mass-loss rate of $4 \times 10^{-9} M_\odot \text{yr}^{-1}$; $V_\infty = 55 \text{ km s}^{-1}$ and $R_* = 166 R_\odot$. We use these parameters because they are better determined than those of single evolved late-type stars. Equivalent width analyses of late-type stars, made where cool star atmospheres attenuate light from a background stellar light source, and from radiative transfer calculations of ζ Aur systems, suggest that $V_{Dopp}/V_\infty \sim 1/3$, (Reimers 1987; Baade 1992).

For the above values $R_W \sim 6 \times 10^6 R_*$ and $R_{ISM} \sim 3 \times 10^4 R_*$. We conclude from this very approximate calculation that the radial extent is bounded by the interstellar medium and that $R_{\tau=1} \sim R_{ISM}$. Since $R_W \gg R_{ISM}$, R_{ISM} depends on the pressure of the interstellar medium (which may vary by a factor of 10) and the product of the mass-loss rate and terminal velocity (which can vary by a factor of 1000). Even with these combined uncertainties, $R_W > R_{ISM}$, and R_{ISM} needs to be calculated for individual stars.

In later M supergiants, the mass-loss rates are higher and the terminal velocities lower, leading to very extended atmospheres. The model for α Ori (M2 Iab) by Hartmann & Avrett (1984) extends to $1600 R_*$. This demonstrates that extended models are needed to study hydrogen under these

conditions. For other atomic models the relevant extent of the atmosphere scales approximately as the abundance relative to hydrogen.

Some models of these evolved stars have been made using a plane-parallel approximation, *e.g.* Ayres & Linsky (1975) and Basri, Linsky & Eriksson (1981). The reason why these and similar models are able to reproduce line fluxes and some line profiles is probably because the emission lines are collisionally excited. The fluxes for these lines scale with the thermodynamic properties as

$$F \propto \int G(T_e) N_e N_H \Delta R, \quad (10)$$

where N_e is the electron density, ΔR is the radial element and $G(T_e)$ is the temperature-sensitive term which includes both atomic and ionization terms, and at chromospheric temperatures increases with T_e . If the chromospheric temperature gradient rises to a maximum within a distance smaller than the stellar radius, the line photons will be created near the stellar surface but these may be scattered in a more extended region where hydrostatic equilibrium no longer holds. In these scattering layers the wind velocity gradient becomes a significant term in the momentum equation (Judge 1990). If the density decreases slowly with height, perhaps due to the passage of waves *bloating* the atmosphere, and the temperature gradient is less steep, then a significant contribution to the total emission-line flux may come from the more extended regions (see for example the empirical calculations for ζ Aur systems by Schröder *et al.* 1988).

2.3 Calculable effects of geometric extension

Inclusion of the radial extension can lead to several changes in computed quantities when compared with results of plane-parallel models. Consider the ionization of hydrogen in an upper chromosphere with a radial extent of $1.05R_*$. This problem is an important one in that N_e is determined by this process and the chromosphere is cooled predominantly by mechanisms that depend linearly on N_e per gram, *i.e.* electron collisional excitation of neutral and singly ionized species and H^- recombination (Ayres 1979). At a given total gas pressure, the electron density can be found from the simultaneous solution of the equations of hydrostatic and statistical equilibrium. If we allow for spherical geometry, the following changes to the equivalent plane-parallel results need to be applied:

- In this region hydrogen is ionized from the $n = 2$ level by the optically thin Balmer continuum. In spherical geometry the radiation will become diluted by a factor F_{dilute}

$$F_{dilute} = 1 - \sqrt{1 - \left(\frac{R_*}{R}\right)^2}. \quad (11)$$

With $R = 1.05R_*$ the Balmer continuum radiation field is reduced by a factor of 1.44 and the ionization rate is also reduced by this factor.

- For simplicity consider an isothermal atmosphere. The equation of hydrostatic equilibrium then becomes

$$N_{tot}(R) = N_{tot}(R \simeq R_*) \exp\left(-\frac{R_*(R - R_*)}{RH_*}\right) \quad (12)$$

where the constant $H_* = H(R_*)$ is the isothermal scale height at the surface of the star. For an evolved star with a surface gravity of 40 cms^{-2} and radius $R_* \sim 60R_\odot$ a radial extent of $1.05 R_*$ is equivalent to $\sim 20 H_*$ at $T_e = 5000 \text{ K}$.

- Inferred emission measures for optically thin lines assume that a given fraction of the photons that are created escape the atmosphere. Typically this is taken as the fraction of the sky that is not occulted by the star. In plane-parallel geometry this fraction $F_{esc} = 1/2$, but in spherical geometry this would be $F_{esc} = (1 - F_{dilute}) \times 1/2$.

Uncertainties in stellar parameters for single stars at distances larger than $\sim 30 \text{ pc}$ are dominated by the uncertainties in the stellar distance and mass. Constraints from parallax measurements, stellar reddening and evolutionary tracks can put limits on these parameters and lead to typical uncertainties of a factor of 2 in the mass and radius. For eclipsing binaries, such as the $\zeta \text{ Aur}$ systems, the stellar parameters are much more secure. Abundances are also uncertain but spectroscopic abundance determinations can also provide an independent surface gravity determination. Atomic data for transitions of interest can have accuracies of 10 per cent for permitted transitions and 25 per cent for intersystem and forbidden transitions. The overall uncertainties in calculated line fluxes are a complicated combination of the uncertainties in atmospheric structure and atomic physics, but analyses that use several different diagnostics can constrain the problem significantly.

In the example of the ionization of hydrogen, for the less extended evolved stars the differences between the results from the different assumed geometries are comparable to the other uncertainties of model atmosphere calculations. Thus in some calculations the more general assumption of spherical geometry should be adopted (*e.g.* Harper 1994).

The situation in more extended chromospheres is clearer. Modelling of wind scattered line profiles can in principle distinguish between the different geometries. Thus the momentum equation (through the gravity) and the geometry requires the modelling of the extended chromosphere/wind regions to be made in spherical geometry. In practice, when using spherical geometry it is often more appropriate to relax the assumption of hydrostatic equilibrium and to solve a specific momentum equation (*e.g.* for a proposed wind mechanism). These momentum considerations are beyond the scope of this paper.

3 MULTI AND S-MULTI

In this section we briefly describe aspects of the code by Carlsson (1986) (MULTI) and describe the modifications made to include spherical geometry. We also mention the main current alternative spherical code, PANDORA (Avrett & Loeser 1984) which has been used in cool stellar atmosphere

calculations where there are no energy constraints imposed. A code (PAM) by Anderson (1992) has recently been published which can treat the spectral effects of millions of lines not in local thermodynamic equilibrium (non-LTE), given energy conservation and hydrostatic equilibrium. This code treats many simplified atomic models simultaneously. However, here we are interested in detailed spectral line formation where more complete atomic models are necessary and the atmosphere may not be static.

MULTI has provided a very powerful tool for studying cool star chromospheres and photospheres. It does *not* assume radiative equilibrium but it is formulated in semi-infinite plane-parallel geometry. The temperature structure of the atmosphere is specified a priori. The code uses a method developed by Scharmer (1981) and Scharmer & Carlsson (1985 a,b) which allows iterative corrections to the population densities to be quickly computed. Approximate operators are used to find approximate corrections to atomic population numbers and the exact rate equations are used to calculate the difference between the approximate and exact solutions, so that the final converged solution is itself exact. MULTI has been updated (Carlsson 1991, 1992) to include the local approximate operator of Olson, Auer & Buchler (1986), Ng acceleration (Ng 1974, *e.g.* see Auer 1987), collisional radiative switching (Hummer & Voels 1988) and the Uppsala Opacity Package, which is based on the opacity program described by Gustafsson (1973). This package allows for the formation of molecules in the number density calculations.

MULTI is clearly structured and readily allows modifications, *e.g.* Uitenbroek (1989a,b) has included the effects of partial redistribution of photons in resonance transitions. Glasse (1989 a,b) and Schmidt & Gesicki (1992) have *reported* spherical versions of MULTI. The latter is contemporaneous with the modifications described here. Glasse adapted MULTI to model submillimetre emission spectra from molecular clouds and this code is available privately (Jeffery 1992). No description of this code has been published.

Most detailed cool star chromosphere/wind calculations (those where the source function is computed from a self-consistent radiation field and not by using escape probability techniques, see Rybicki 1984) in spherical geometry have been made with the PANDORA code (Avrett & Loeser 1984, 1992; Luttermoser 1992). PANDORA is a large program and contains many physical options which allow a wide range of stellar atmosphere problems to be tackled; *e.g.* velocity fields can be included in the statistical equilibrium equations. To date, however, PANDORA has not been used by many independent investigators, whereas MULTI is in widespread use throughout the astrophysics community.

The modifications described here have been made to the recent version of MULTI and the addition of spherical geometry removes one of the disadvantages of using MULTI compared with PANDORA. Avrett & Loeser (1984) describe the spherical scheme for PANDORA and present a comparison with previous spherical schemes. We extend these to include results from the scheme adopted in S-MULTI.

3.1 Computing requirements

The dominant memory requirement in MULTI scales with n_τ , the number of optical or spatial depth-points and n_l , the number of atomic levels. For the global operator version, the dominant memory requirement scales as $n_\tau^2 n_l^2$ (Carlsson 1991), which reflects the physical coupling of every atomic level with every other atomic level everywhere in the atmosphere. In S-MULTI the atomic parameters are stored on the same atmospheric grid as in MULTI so there is no direct increase in memory requirement. Some problems, however, require more depth-points because of either the increased opacity (and spatial) range present in cool winds or the presence of macroscopic velocity fields. In the local operator version of MULTI the memory scales as $n_\tau n_l^2$. Thus for more extended atmospheres and wind models the local operator version is more attractive. The converged solution, however can take many more iterations and increases the total computing time for a given problem (Carlsson 1992). The number of iterations required for convergence depends mostly on the starting approximations for the atomic level populations.

The main computational overheads for spherical over plane parallel geometry are the number of rays required to sample the spatial volume and the storage of frequency information. The formal solution is made for each frequency-angle at each iteration and if these dominate the total computing time, then the total time will scale with the number of rays. Typically there may be a factor of ~ 30 more rays in a spherical model compared to a plane-parallel model. However, rays which intersect shells at greater radial distances have less points along them, which reduces this overhead. In moving atmosphere calculations the angles and frequencies are coupled which leads to large temporary files containing the profile information for each frequency-angle.

3.2 Physical Scales

Spherical symmetry is one-dimensional because all of the physical parameters are specified in one coordinate only, namely the radius. However, the physical problem now has two natural scales. The first, in common with the plane-parallel case, is the optical depth-scale, which is used to determine the formal solution to the radiative transfer equation. The second is the height-scale, which gives the geometry of the atmosphere. The choice of a discrete atmospheric grid on which the calculations are made is more critical because of spatial (angle) quadratures of the intensity and flux. In the presence of mass flows this becomes even more important because of the need to adequately sample the velocity field. Most of the modified subroutines in S-MULTI deal with the input and output of the height-scale, which was not used as input in MULTI. Normalized opacities are used throughout both codes, where the reference opacity is at $\lambda 5000\text{\AA}$ and the reference optical depth-scale is $\tau_{\lambda 5000}$. The height-scale is defined such that the stellar radius R_* is the radial distance where $\tau_{\lambda 5000} = 1$. Stellar line fluxes, F_* , are most often derived from the fluxes observed at the Earth, F_\oplus , and the photospheric angular diameter, ϕ , through the relation $F_* = F_\oplus (2/\phi)^2$. To specify fluxes in spherical geometry requires a specific radial distance. In S-MULTI to aid comparison with observations we give the flux as if it were projected on to the star at a radius of R_* . This is appropriate if the optical angular diameter corresponds to this same radius. These conventions need to be borne in mind when comparing S-MULTI models with other semi-empirical atmospheric models (such as eclipse models) and model photospheres (*e.g.* see the discussion in Baschek *et al.*

1991).

3.3 Spatial grid

To evaluate the integrals that contain the specific intensity, I_ν , at a frequency ν , *e.g.* the mean-intensity J_ν and line flux F_ν , we need to specify along which directions, or rays, I_ν is calculated. In the following, the angle between the normal to the atmosphere (radial vector) and a given ray is θ and $\cos \theta = \mu$. Fig. 1 shows the location of the rays in plane parallel (a) and spherical geometry (b).

The depth-points, k increase inwards from the outer tenuous atmosphere towards the bottom boundary (photosphere). The formal solutions are made for the rays, labelled mu , and the angular information of the radiation field is provided by the distribution of rays. The depth-scale for the atmosphere is specified for each problem and is chosen to restrict the location of the rays for which formal solutions are computed. The rays that sample the spatial volume of the atmosphere either intersect the core (as in plane-parallel geometry) or pass through the whole atmosphere. The rays that intersect the core are chosen so that they are evenly spaced in μ at the core. The rays that pass through the atmosphere are specified such that each ray becomes the tangent to a shell of a radius that corresponds to the radial distance of a depth point. The grid along each ray consists of all the intersections with shells of greater radii. This choice is convenient since the atmospheric parameters are already specified at each point along each ray. This type of grid is also known as a P-Z grid where the impact parameters, P, are chosen to correspond to the radial distance of all the depth-points. Thus the total number of rays, nmu , is all those that intersect the core $ncore$ plus the number of depth-points $ndep$. The number of points along each ray is $ndepk$, so for rays $mu = 1$ to $mu = ncore + 1$ each ray intersects all of the atmospheric depth-points, *i.e.* $ndepk = ndep$ but for $mu > ncore + 1$, $ndepk < ndep$.

Other P-Z grids could be chosen, for example Nordlund (1984) suggests a different grid for *each* frequency to permit accurate evaluation of the intensity integrals. The calculation of the geometric terms is fast and helps to treat the characteristic forward-pointing radiation field. In this case, an interpolation scheme is required to calculate the atmospheric parameters at the tangent for each ray which does not intersect a prescribed depth-point.

The implementation of spherical geometry in S-MULTI is done simply by scaling the optical depth-between two depth points along the radial ray by a factor that depends on the angle of the rays mu . This gives the optical depth between the same grid-points for each ray. The disc centre ray, ($mu = 1$), is the reference direction and the optical depth between any two points, k and $k + 1$, along another ray, mu , is then (in terms of normalized opacities)

$$\Delta\tau_{\nu, mu, k} = \frac{C(mu, k + 1)}{2} \cdot \left(\frac{\kappa_{\nu, mu, k}}{\kappa_{\lambda 5000, k}} + \frac{\kappa_{\nu, mu, k+1}}{\kappa_{\lambda 5000, k+1}} \right) \cdot \Delta\tau_{\lambda 5000, \mu=1, k} \quad (13)$$

where the array of weights, $C(mu, k + 1)$, is a function of angle and depth-point and is calculated once and applies for all frequencies. κ is the total monochromatic opacity and $\kappa_{\lambda 5000}$ is the reference opacity for the frequency corresponding to $\lambda = 5000 \text{ \AA}$. In plane-parallel geometry $C(mu, k + 1) =$

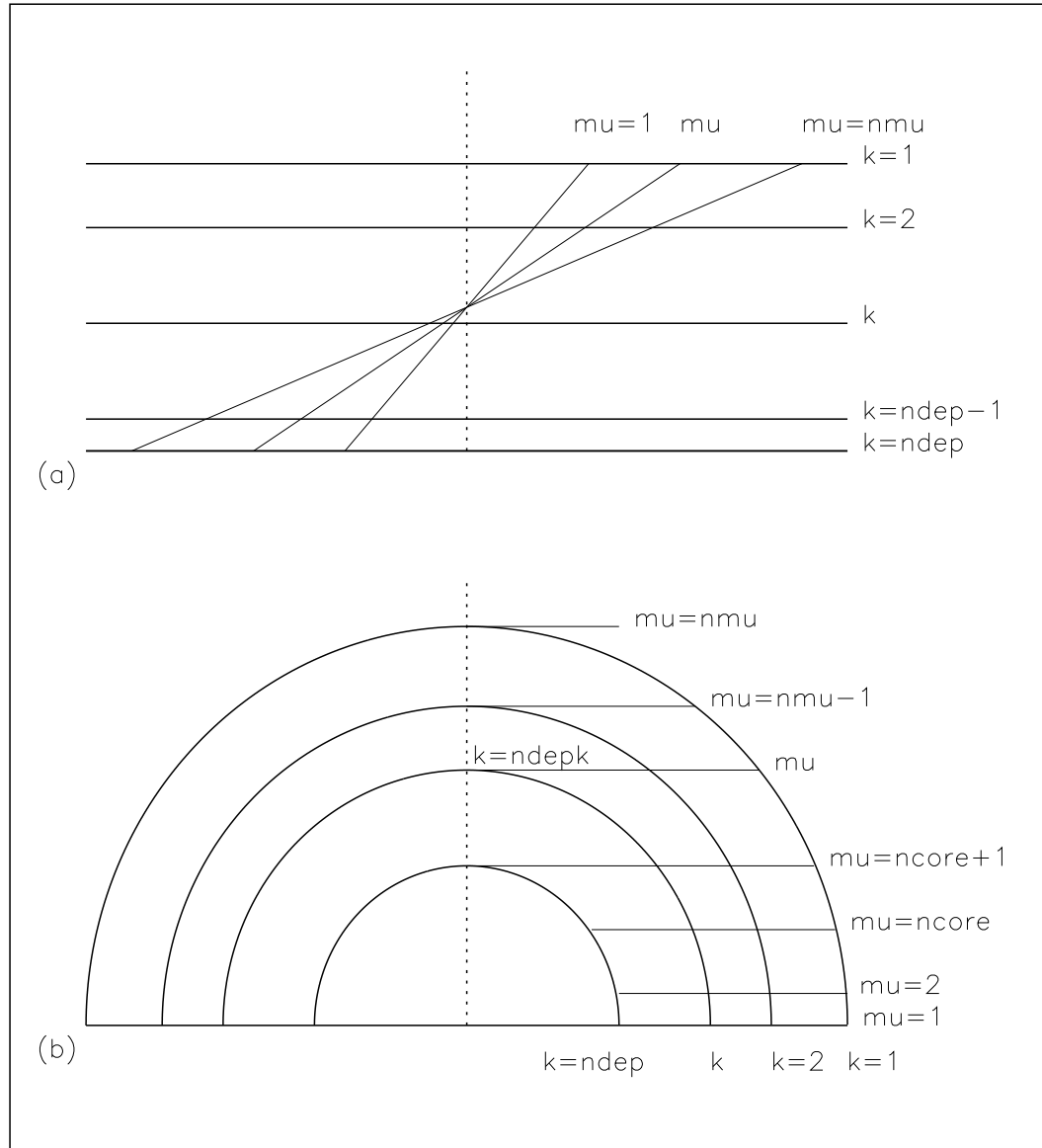


Figure 1: Schematic diagram showing the placement of rays in different geometries: (a) plane-parallel, and (b) spherical symmetry. The maximum number of atmospheric depth-points, k , is $ndep$, and the number of atmospheric grid-points along a ray is $ndepk$. The maximum number of rays, μ , is nmu and the number of rays that intersect the opaque core at angles less than $\pi/2$ is $ncore$. In plane-parallel geometry $ndepk = ndep$ for all rays and in spherical geometry $ndepk = ndep$ for $\mu \leq ncore + 1$ and $ndepk$ is less for the other rays. The atmospheric grid is where the depth shells (or layers) intersect the rays, *i.e.* the number of intersections decreases with increasing μ . Notice that the angle between a ray and the layers in plane-parallel geometry is the same for all depths, while in spherical geometry the angle is a function of ray and depth-point.

$1/\mu$ and is independent of the depth in the atmosphere. The simplest way to calculate the weights is to assume that the optical depths scale as the geometrical path-length. This scaling is not *exact* since the increments $\kappa(R)dR$ are not linearly scaled from those along the reference ray. If the opacity is monotonically increasing towards the stellar surface then the optical depths calculated geometrically will *under-estimate* the true optical depths. If a model for the opacity distribution is known in advance *e.g.* that implied by equation (3) and if the cross-section per hydrogen atom is constant, then $C(mu, k + 1)$ can be determined from that particular distribution. Appendix A shows how to calculate $C(mu, k + 1)$ for this case.

In general, however, the opacity for a particular frequency is a complicated convolution of atmospheric and atomic physics and does not lend itself to simple analytical representation. In most of the comparison test cases below, and in S-MULTI, we use the geometric weights for $C(mu, k + 1)$. The difference between the weights, $C(mu, k + 1)$, for the geometric method and for the example in the test cases are estimated in Section 4.2.1 and Appendix A.

3.4 Calculation of the opacity scale

$\kappa_{\nu, mu, k} / \kappa_{\lambda 5000, mu, k}$ normally varies more slowly with height than does $\kappa_{\lambda 5000, mu, k}$ since the opacities scale approximately together with the density. From equation (13) it can be seen that the conversion of the input height-scale to $\tau_{\lambda 5000}$ scale is important. Solutions to the momentum equation for stellar atmospheres are given in terms of radius and density. These are a natural choice for input into the radiative transfer code. In S-MULTI, $\tau_{\lambda 5000}$ is computed using the height-scale and $\kappa_{\lambda 5000}$. Logarithmic integration has been adopted to compute $\tau_{\lambda 5000}$ from the given R and N_H scales. Again this opacity scale may be calculated directly from a model opacity distribution.

3.5 The observer's frame

MULTI is coded in the observers frame and we keep this reference frame in S-MULTI. The velocity fields in cool star winds are poorly known. However, in flows where the observed terminal velocity is less than the surface escape velocity, as is often observed (Baade 1990), little momentum is added to the flow beyond several stellar radii. The flow may then decelerate under the influence of gravity so the flows may be non-monotonic. Pulsations also lead to non-monotonic velocity fields. Microturbulent motions present in stellar atmospheres contribute to the broadening of the atomic line profile, and as can be seen below the relative size of the macroscopic velocity field compared to the microturbulent velocity is an important factor in calculations of moving atmospheres. The relation between atmospheric turbulence or stochastic motions and the classical microturbulence is unknown. It is often assumed that observed non-thermal line broadening of disc integrated optically thin lines sets an *upper* limit to the classical microturbulence. The one-dimensional nature of the problem means that only radial velocity fields can be described. Since most stars are rotating with respect to the actual observer's frame the atmosphere may have non-radial velocity fields present. The angular velocity fields are determined by the torque exerted on the flow. Fortunately, the angular velocities for late-type stars (for spectral type G0, $\langle v \sin i \rangle \simeq 5$ to 8 km s^{-1} and decreases with later spectral type, Gray 1992) in most cases are comparable to typical values of the

microturbulence in the chromosphere. In this case we assume that the effects of stellar rotation can be ignored. For stars that rotate more rapidly, if the region of interest is co-rotating, then the solution will be a good approximation in this frame. The flux profile can then be generated by convolution of the calculated intensities with the stellar rotation profile.

An important problem in calculations that including velocity fields is that the frequencies and angles are coupled. In the static case, a photon at line centre in the observers frame will also be at line centre with respect to the plasma. When the gas is moving, the atomic line profile (moving with the flow) is Doppler shifted with respect to the observer's frame. Consider Fig. 2, where a ray becomes a tangent to a shell, the atomic line profile (which determines the opacity and emissivity at a given frequency) has no Doppler shift in the observer's frame. At the next point along the ray, the atomic line profile will have a Doppler shift of $V \cos \theta$.

In this example there is an outflow of constant velocity V and microturbulence V_{micro} such that $V = 3V_{micro}$ and a Doppler broadened atomic line profile. If we set the maximum Doppler shift between grid-points to a suitable upper limit of $0.5V_{micro}$ (Cannon 1985; Mihalas 1978) then the angle θ must satisfy $\cos \theta \leq 1/6$. If we then construct the depth-scale with $ndep$ depth-points, using this criterion, then $R_2 = R_1 \cdot \sin \theta$ etc, where $k = 1$ is the outermost point.

Then

$$\frac{R_1}{R_{ndep}} = \left(\frac{1}{\sin \theta} \right)^{ndep-1}. \quad (14)$$

Thus for an atmosphere thus has a total radial extent of $30R_{ndep}$, where $k = ndep$ is the innermost point, then $ndep = 243$, which is currently computationally restrictive. This atmospheric extent is sufficient for the chromospheres of coronal stars but not necessarily for non-coronal stars. Allowing larger angles can lead to poor accuracy in the optical depth-scale along the ray. To circumvent this problem we interpolate points between the tangent and the next point to reduce the Doppler shift between adjacent points (see below).

3.6 Interpolation at the tangent

To avoid the possibility of the poor sampling of line opacity mentioned above, we add additional points between the tangent and the adjacent grid points. This scheme has been adopted in other spherical codes (Avrett & Loeser 1984; Baade 1992). Fig. 2 illustrates the inclusion of two interpolation points along the ray mu . They are located between the tangent grid point, $k + 2$ and the adjacent point, $k + 1$. Following Avrett & Loeser, the i points are located, in this case, such that

$$R_i = R_{k+2} + \left(\frac{1}{2} \right)^i (R_{k+1} - R_{k+2}) \quad i = 1, 2, \dots, nintep \quad (15)$$

where there are $nintep$ points (here $nintep = 2$) and the use of i is to distinguish these points from the atmospheric, k grid. The total number of grid-points along this ray is now $= ndepk + nintep$. The main purpose of this procedure is that the $\Delta \cos \theta_i$ s are significantly less than $\Delta \cos \theta$ at the tangent.

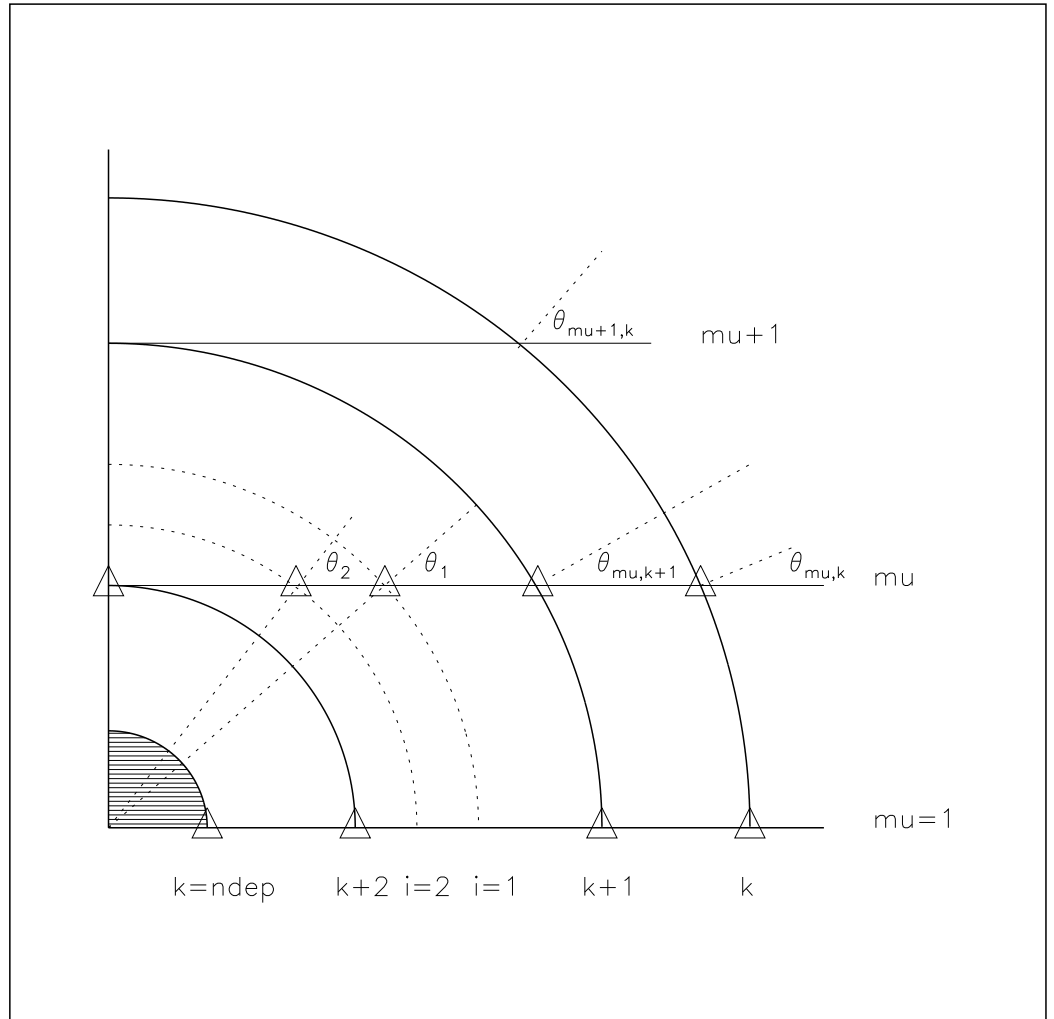


Figure 2: Schematic diagram showing the interpolation scheme for a grazing ray. The interpolated points, i , are between $k + 1$ and $k + 2$. The number of interpolation points, n_{intep} , here is two. The interpolation occurs between the final and penultimate points along each ray. Measured along the radial ray ($mu = 1$) the distance between the shells $i = 1$ and $i = 2$ is half of that between $i = 1$ and $k + 1$. The interpolation points are located where the shells, i , intersect the ray in question; these intersections plus the normal grid points are shown as triangles. Note how in a moving atmosphere the projected velocity along the ray is reduced more slowly to zero at the tangent. Rays that intersect the core also have interpolation points and are located in a similar fashion.

3.7 Quadratures

3.7.1 Spatial quadratures

In S-MULTI we adopt trapezoidal quadrature (also adopted by Avrett & Loeser 1984). MULTI uses Gaussian quadrature for the angle integrals because the angles of the rays to the normal are the same for all depth-points, enabling both the angles and weights to be chosen as to optimize the *accuracy* for a given number of rays. Thus for trapezoidal quadrature more rays are required to intersect the core, compared with Gaussian quadrature. Also, separate weights are used for the flux integrals. In Gaussian quadrature the same weights are used in both the intensity and flux integrals (see Sykes 1951).

3.7.2 Frequency quadrature

One further requirement often discussed in this context is that the frequency grid should also be sufficiently wide to be extended by $\pm 3V_{wind}/V_{micro}$ over the static case. In the context of cool star atmospheres, the frequency grids are often very broad because the resonance lines have significant opacity broadening. Indeed, the presence of scattering by the stellar wind can be observed *within* the broad emission-line profiles (*e.g.* Reimers 1982; Drake, Brown & Linsky 1984).

3.8 Formal solution of the radiative transfer equation

In MULTI the radiative transfer equation is solved as a second-order differential equation with two boundary conditions. The Feautrier method is used to solve the finite-difference equations. In MULTI (S-MULTI) the algorithm for the formal solution takes advantage of a numerical conditioning technique by R. F. Stein (see Nordlund 1982). Good accuracy is obtained when the grid has a constant $\Delta \log \tau$ and samples the changes in the monochromatic source function. The mean intensity, which is used in the rate equations, requires the integral of the specific intensity over solid angle.

3.8.1 Boundary conditions

In the semi-infinite atmosphere problem treated in MULTI, the outer boundary condition assumes that there is no incident radiation at $\tau = 0$. Incident radiation from an external source could be included, if necessary. Allowance is made for the finite optical depth of the outer boundary, by assuming that the source function remains constant from $\tau_{k=1}$ to $\tau = 0$. In plane-parallel geometry the optical path length for this correction is simply

$$\tau_{\mu} = \frac{\tau_{\mu=1}}{\mu}, \quad (16)$$

where $\tau_{\mu=1}$ is the optical depth along the normal. In spherical geometry this is no longer strictly

valid (see Section 3.3 and Appendix A). We have assumed that the opacity follows the density profile implied by equation (3). For this distribution we obtain

$$\tau_\mu = \tau_{\mu=1} \frac{\theta}{\sin \theta}, \quad (17)$$

where $\theta = \cos^{-1} \mu$ rad. When $\theta = 0$ we have $\tau_\mu = \tau_{\mu=1}$ and when $\theta = \pi/2$ $\tau_{\mu=0} = \tau_{\mu=1} \pi/2$. Whereas the plane-parallel assumption leads to $\tau \rightarrow \infty$ as $\mu \rightarrow 0$.

The case of $\theta = \pi/2$ has been examined previously in studies of eclipsing systems. These considered the relation between the density at the tangent to the total line-of-sight column density (the column density along the radial ray being found analytically). For example the analysis of the solar chromosphere during eclipses (Menzel 1931). Various density profiles have been considered in the study of symbiotic systems (Islaker, Nussbaumer & Vogel 1989, Vogel 1991) and approximate analytical solutions have been found for exponential opacity distributions for the ζ Aur and ϵ Aur binary systems (see Menzel *circa* 1936; Kuiper, Struve & Strömberg 1937, respectively).

At the photospheric boundary a diffusion approximation is adopted using the gradient of the monochromatic source function.

3.8.2 Symmetry conditions

In spherical geometry, rays that do not intersect the core require different boundary conditions. In a static atmosphere the Feautrier intensity variable, P , at depth point, k , is (Mihalas 1978)

$$P_{k,mu,\nu} = \frac{1}{2} [I_{k,mu,\nu} + I_{k,-mu,\nu}]. \quad (18)$$

By symmetry $I_{ndepk+k,mu,\nu} = I_{ndepk-k,-mu,\nu}$ where $ndepk$ is the depth point where the ray is a tangent to the corresponding shell (see Fig. 1), so we need only solve the rays for the half-atmosphere. Since there is no coupling between the frequencies and angles, we also only need to consider the half-line profile since the atomic line profile is symmetric about line centre.

In the moving atmosphere, the Doppler shifting of opacity is only considered for line transitions. For bound-free transitions the Feautrier variable is that given in equation (18). For bound-bound transitions the Feautrier variable has the less symmetrical form

$$P_{k,mu,\Delta\nu} = \frac{1}{2} [I_{k,mu,\Delta\nu} + I_{k,-mu,-\Delta\nu}] \quad (19)$$

where $\Delta\nu$ is the frequency displacement from line centre. Here the full length of the ray needs to be solved, because P is no longer symmetrical in the atmosphere for a given frequency. The far boundary condition is then the same as the outer boundary condition. Whereas in the static case only half of the line profile needs to be considered, in moving atmospheres the full profile must be calculated. However, we can store the information for the extra half of the ray and assign it to the

symmetric frequency point in the forward half of the ray. The rays that intersect the core must be solved for all frequencies since this symmetry does not exist.

3.9 Approximate operators

The approximate correction for the population numbers is based on an approximate solution of the transfer equation. The exact rate equations are combined with these approximate solutions such that the converged solution is exact. The approximate solution to the transfer equation is made using approximate operators.

MULTI contains two forms of approximate operator. One makes *global* corrections to the population densities and is based on an approximate integral solution of the transfer equation (see Scharmer 1984) and the other is a purely *local* (diagonal) operator, based on the second-order finite difference transfer equation (Olson *et al.* 1986).

3.9.1 The Scharmer approximate global operators

The formal solution of the radiative transfer equation

$$\frac{dI}{d\tau} = I - S \quad (20)$$

along each ray can be written as an operator equation

$$I^\pm(\tau) = \Lambda[S(\tau)] \quad (21)$$

and the approximate solution can be written

$$I^\pm(\tau) \simeq \Lambda^\dagger[S(\tau)] \quad (22)$$

where I^+ is the intensity from outgoing ray and I^- is the intensity from the incoming ray. Λ is the lambda operator and Λ^\dagger is an approximate operator.

The intensity from outgoing, $\mu > 0$, and incoming, $\mu < 0$, rays for a ray of total optical depth, T , is given by

$$I^+(\tau) = e^\tau \int_\tau^T S(\tau') e^{-\tau'} d\tau' ; I^-(\tau) = -e^\tau \int_0^\tau S(\tau') e^{-\tau'} d\tau' \quad (23)$$

where there is no incident radiation at the boundaries. Note that here $\tau = \tau_{ref}/\mu$, where τ_{ref} is the reference scale, so that $\tau < 0$ when $\mu < 0$.

3.9.2 Asymmetric atmospheres; semi-infinite and slab geometries

The global approximate operator employed in MULTI is based on the Eddington-Barbier relationship from a source function of the form

$$S(\tau) = a + b\tau. \quad (24)$$

This form is robust and has a reasonable functional form for smooth structures. This representation is evaluated for both incoming and outgoing rays for each frequency-angle. The approximate solution is written as

$$I^\pm(\tau) = \omega^\pm S(\tau^\pm) \quad (25)$$

where ω^\pm are the quadrature weights and τ^\pm are the quadrature points. Scharmer (1984) derived these quantities for both semi-infinite and slab geometries. Consider the finite slab of total optical depth T . Substituting equation (24) into equation (23) we obtain

$$I^+(\tau) = (1 - e^{-\delta\tau}) \left[a + b \left(1 + T - \frac{\delta\tau}{1 - e^{-\delta\tau}} \right) \right] \quad (26)$$

and

$$I^-(\tau) = (1 - e^{-\tau}) \left[a + b \left(1 + \frac{\tau}{1 - e^{-\tau}} \right) \right]. \quad (27)$$

Comparing equations (26) and (27) with (25) we find

$$\omega^+ = 1 - e^{-\delta\tau} ; \quad \tau^+ = 1 + T - \frac{\delta\tau}{\omega^+} \quad (28)$$

and

$$\omega^- = 1 - e^{-\tau} ; \quad \tau^- = \frac{\tau}{\omega^-} - 1 \quad (29)$$

where $\delta\tau = T - \tau$. When $T \rightarrow \infty$ the incoming ray quadrature point and weight remain the same and the outgoing quantities become

$$\omega^+ = 1 \quad :: \quad \tau^+ = 1 + \tau. \quad (30)$$

This is the semi-infinite atmosphere form employed in MULTI. Notice now that τ^+ is a monotonically increasing function of τ , leading to an efficient search for the quadrature point in the atmospheric model. For each optical depth, τ , along the ray there is a corresponding quadrature point, τ^+ . Because the optical depth measured from the observer along the ray increases along the computational grid, we know that if the weight $\tau^+(k)$ corresponds to point $\tau(k)$, then we need only search for $\tau^+(k+1)$ starting from $\tau^+(k)$.

3.9.3 Approximate operator for spherically symmetric finite atmospheres

The above procedure can be repeated but now allowing for the symmetry of the atmosphere. For a ray of total optical depth, T , which passes through the whole static spherically symmetric atmosphere (*i.e* a ray which does not intersect the stellar core) the monochromatic source function must also be symmetric about the mid-point $\tau = T/2$. The source function can now be approximated by the form

$$S(\tau) = \begin{cases} a + b\tau, & \text{when } \tau \leq \frac{T}{2}; \\ a + b(T - \tau), & \text{when } \tau \geq \frac{T}{2}. \end{cases} \quad (31)$$

Substituting these into equation (23) we obtain

$$I^+(\tau) = (1 - e^{-\delta\tau}) \left[a + b \left(\frac{\tau + 2(1 - e^{T/2}e^{-\delta\tau})}{1 - e^{-\delta\tau}} - 1 \right) \right], \quad (32)$$

and mapping onto the atmosphere where $\tau \leq T/2$, then gives

$$\omega^+ = 1 - e^{-\delta\tau} \quad \therefore \quad \tau^+ = \frac{\tau + 2(1 - e^{T/2}e^{-\delta\tau})}{\omega^+} - 1, \quad (33)$$

where $\delta\tau = T - \tau$. These quadrature points and weights supply the information about the symmetry.

The condition that τ^+ is monotonically increasing with τ is no longer valid because we have used the symmetry to map the quadrature points on to the atmosphere where $\tau \leq T/2$. Examination of $d\tau^+/d\tau$ for the static case, however, provides a search strategy for finding the quadrature points. When $d\tau^+/d\tau$ is positive the search can progress monotonically, as before. $d\tau^+/d\tau$ becomes zero when $\tau^+ = \tau$ and then τ^+ declines until $\tau = T/2$. $\tau^+(T/2)$ can be determined analytically. The maximum of τ^+ is the solution to

$$e^T = e^{\tau^+} [2e^{T/2} - (\tau^+ + 1)] \quad (34)$$

which can be found algebraically and is quickly solved by a Newton-Raphson iteration cycle. The search could proceed as follows

- Monotonically search for τ^+ until $\tau^+(\tau) = \tau_{max}^+$
- Then search *from* $\tau^+(T/2)$ for the remaining τ^+ .

In practise the search for the maximum value of τ^+ is not justified and it is quicker to search monotonically until $\tau^+(\tau) = \tau^+(T/2)$ and afterwards continue to search from this point.

The quadrature points found from the Scharmer operators generally lie between two grid-points. The choice of a linear source function representation lends itself naturally to a linear interpolation scheme to proportion the population corrections to the adjacent grid-points (Scharmer 1984). Because the corrections do not need to be exact, this linear representation does not affect the accuracy of the final solution.

In the presence of velocity fields the grazing ray is solved in its full length. The monochromatic source function is no longer symmetric about the axis of symmetry. The following scheme is adopted in this case. The corrections are applied for the first half of the atmosphere as above. In the second half of the atmosphere we proceed inwards from the outermost point and assign the corrections to the symmetric frequency point.

3.9.4 Local operator

Although the spherical version does not increase the dominant memory requirements of the code directly, the increase in the number of depth points needed in extended models will lead to an increase in the required memory. In addition, in the very low densities of the outer atmosphere, double precision may be needed. The implementation of the local operator of Olson *et al.* (1986) leads to a lower memory requirement at the cost of increased number of iterations. We have found, as have others (Puls & Herrero 1988), that this operator has excellent properties, being robust and leading to optimum convergence rates. We have found that other forms of this operator which estimate the Feautrier intensities in adjoining regions in a different manner also have favourable convergence properties. The local Feautrier ‘mean’ intensity, $P = (I^+ + I^-)/2$, sampling of Olson *et al.* (1986) is determined by the separation in optical depth between the adjacent grid-points,

$$P_{k-1} = P_k e^{-\Delta\tau_k} \quad (35)$$

We have found that in the test cases described below, Feautrier intensity sampling which has a less rapid decline with $\Delta\tau_k$ can lead to *enhanced* convergence rates. The following sampling is such an example:

$$P_{k-1} = P_k \cdot \frac{1}{1 + \Delta\tau_k} \quad (36)$$

This form of sampling satisfies realistic physical limits for the adjoining Feautrier intensities, *i.e.* $P_{k-1} \rightarrow P_k$ as $\Delta\tau_k \rightarrow 0$ and $P_{k-1} \rightarrow 0$ as $\Delta\tau_k \rightarrow \infty$ and the local operator $\Lambda^\dagger \rightarrow O(\Delta\tau_k)$ as $\Delta\tau_k \rightarrow 0$ and $\Lambda^\dagger \rightarrow 1$ as $\Delta\tau_k \rightarrow \infty$. The approximate local operator, in this case is

$$\Lambda^\dagger = \left[1 + \frac{1}{\Delta\tau_{k+1/2}} \left(\frac{1}{1 + \Delta\tau_k} + \frac{1}{1 + \Delta\tau_{k+1}} \right) \right]^{-1}. \quad (37)$$

Note that the approximate local operators described by Rybicki & Hummer (1991) could be straightforwardly implemented within MULTI (S-MULTI).

3.10 Electron densities

For a given total number of particles it is possible to find a self-consistent solution for the ionization of hydrogen and the electron density. In plane-parallel geometry there is a convenient relation from the hydrostatic momentum equation between the mass-column density, $mcol$ and the total pressure, which is the sum of turbulent, gas and radiation pressures, $P_{tot} = P_{turb} + P_{gas} + P_{rad}$:

$$P_{gas} + P_{turb} + P_{rad} = mcol \cdot g_*. \quad (38)$$

In spherical geometry or non-static atmospheres this relation does not hold. In MULTI, the input depth-scales are either $\tau_{\lambda 5000}$ or the mass column density. When solving for the electron density, the above relation (without the radiation pressure term) is used to find the total number of particles. In S-MULTI, the density is now given as input, *i.e.* the momentum equation is no longer solved, and the total number of hydrogen atoms is thus specified. The density can be given either in terms of the mass-loss rate, assuming constant time-independent outflow, or given explicitly. In both cases the charge conservation equation and the ionization of hydrogen are solved iteratively to find a self-consistent solution for the electron densities, keeping the total mass density constant.

3.11 Fixed radiative rates

It is sometimes convenient to fix some of the radiative rates in the statistical equilibrium equations (rate equations). MULTI includes the option to prescribe photoexcitation or photoionization rates via a given radiation temperature, as described by Auer, Heasley & Milkey (1972). The *spirit* of these approximations has been included in S-MULTI where the radiation dilution has been included in the excitation rates and the stimulated emission terms. In essence, the radiation temperature can be set equal to the electron temperature where the radiation field is thermalized, and then to a fixed value representative of the temperature where the radiation field becomes optically thin. In S-MULTI the radial distance of this transition from optically thick to optically thin photoionizing radiation fields is used to determine the radiation dilution factor outside this transition zone.

4 COMPARATIVE TEST CALCULATIONS

In this section we compare the results of some idealized calculations, made with the scheme outlined above, with previous investigations. These numerical comparisons are necessary because of the absence of analytical results for these types of radiative transfer problems.

The first part gives a comparison of our results with those presented by Avrett & Loeser (1984); Rogers (1984) and the previous investigations they discuss. These calculations test (i) the angular quadrature weights and (ii) the matrix elements of $C(mu, k + 1)$ (iii) the formal solution of the radiative transfer equation which includes the boundary conditions for the grazing rays and (iv) the grazing ray interpolation scheme. These cover the essential modifications to MULTI that are included in S-MULTI and provide an indication of accuracy. The second part examines the effects

on the solutions of both the grid spacings and the interpolation scheme. These latter investigations demonstrate the sampling requirements in the same idealized moving atmosphere case as described in the first part of this section and are aimed at giving other investigators who use S-MULTI an idea of the sampling requirements for more realistic radiative transfer problems.

4.1 Avrett & Loeser (1984) and Rogers (1984)

Avrett & Loeser (1984) describe line transfer in expanding atmospheres and also compare their results with those found by other investigators. Their computer code forms part of the PANDORA program. To make the comparison with the results presented in their paper we have used the scheme outlined above to treat idealized test cases. There are four test cases (we have not included *partial-redistribution* in the S-MULTI observer frame code). Of these, three are for static atmospheres and one is for an expanding atmosphere. Rogers (1984) also discusses the solution of line transfer problems using a half-range moment method described by Martin, Rogers & Rybicki (1984) and Rogers & Martin (1984). This method is best suited to static atmospheres, and we include these static atmosphere results in our comparisons. These four comparison cases are

1. Static atmosphere: Monochromatic Scattering.
2. Static atmosphere: Line transfer with frequency-independent background source function.
3. Static atmosphere: Line transfer with frequency-dependent background source function.
4. Expanding atmosphere: Line transfer with frequency-independent background source function.

Cases 1–3 test the optical depth weights, quadrature weights, book-keeping, and the grazing ray symmetric boundary condition, while case 4 tests the moving atmosphere boundary condition and the viability of the tangent ray interpolation scheme in improving the accuracy of the grazing ray formal solutions and hence the line profiles.

4.1.1 Specification of the line formation problem

Here we adopt notation such that (AL-23) refers to equation (23) of Avrett & Loeser (1984). We also work in terms of the dimensionless frequency variable x , a normalized frequency variable defined such that the normalized lined profile is given by

$$x = \frac{\nu - \nu_0}{\Delta\nu_{Doppl}} \quad \text{and} \quad \varphi(\nu) = \frac{\phi(x)}{\Delta\nu_{Doppl}}, \quad (39)$$

where $\Delta\nu_{Doppl}$ is a characteristic Doppler width which is taken as constant throughout the atmosphere and ν_0 is the line centre frequency. $\phi(x)$ is given by equation (48).

The monochromatic source function at a given point (dropping the grid subscript) can be written as

$$S_x = \frac{\phi(x)\kappa_L S_L + \sigma J_x + \kappa_A S_A}{\phi(x)\kappa_L + \sigma + \kappa_A} \quad (40)$$

where S_L is the frequency-independent line source function, here we assume *complete redistribution*, and S_A is the continuous absorption source function. Then the continuous opacity is comprised of pure absorptions κ_A and coherent scattering σ . Both of these are assumed to be constant over the line profile. κ_L is the frequency-independent line opacity.

J_x is the mean intensity, which in a spherically symmetric geometry can be written as

$$J_x = \frac{1}{2} \int_{-1}^{+1} I_{x,\mu} d\mu \quad (41)$$

where I_x is the specific intensity and μ is the cosine of the angle between the particular ray and the normal to the atmosphere (the radial vector).

The statistical equilibrium equations allow the line source function to be written in the following form (for example, see Mihalas 1978):

$$S_L = \frac{\bar{J} + \epsilon B_x}{1 + \epsilon} \quad (42)$$

where

$$\bar{J} = \int_{-\infty}^{\infty} \phi(x) J_x dx \quad (43)$$

and J_x is the frequency-dependent mean intensity which is calculated from the self-consistent solution of the equations of statistical equilibrium and radiative transfer. B_x is a source term. In the example of a two-level atom, B_x is the Planck function and ϵ is given by

$$\epsilon = \frac{N_e C_{21}}{A_{21}} (1 - e^{-h\nu_0/kT}) \quad (44)$$

where levels 1 and 2 are the lower and upper levels respectively and $h\nu_0$ is the energy difference between the levels. C_{21} is the collisional de-excitation rate per electron per atom and A_{21} is the Einstein spontaneous decay coefficient. In a more complete atomic model, B_x and ϵ will contain additional terms but the form of S_L will be the same. It remains to specify the particular values for the parameters described above, for each comparative case.

Table 1: Atomic parameters for comparison with Avrett & Loeser (1984)

Parameter	Case 1	Case 2	Case 3	Case 4
S_A	1.0	1.0	1.0	1.0
$J_{x,c}$	$J_x \equiv J_{x,c}$	$J_{x,c}$	J_x	$J_{x,c}$
B_x	N/A	1.0	1.0	1.0
κ_A	†Eq(46)	†Eq(46)	†Eq(46)	†Eq(46)
σ	†Eq(46)	†Eq(46)	†Eq(46)	†Eq(46)
κ_L	N/A	†Eq(47)	†Eq(47)	†Eq(47)
ϵ	N/A	2×10^{-3}	2×10^{-3}	2×10^{-3}
$\phi(x)$	N/A	†Eq(48)	†Eq(48)	†Eq(48)

N/A : Not Applicable

† The equation for this parameter is given in the text

4.1.2 Specifications of atomic parameters

In the following cases the monochromatic continuum scattering mean intensity (hereafter known as $J_{x,c}$) is either calculated self-consistently *i.e* it is the same J_x as that used to calculate \bar{J} in the line source function in equation (43), or for convenience it is taken to be the mean intensity from the solution of case 1. In the latter instance, equation (40) then becomes

$$S_x = \frac{\phi(x)\kappa_L S_L + \sigma J_{x,c} + \kappa_A S_A}{\phi(x)\kappa_L + \sigma + \kappa_A} \quad (45)$$

where all other definitions remain the same. The atomic parameters used in the four test cases are given in Table 1.

The opacities and line profile used here are defined below:

$$\kappa_A = \sigma = \frac{60}{29} \cdot \frac{1}{R^2}; \quad (46)$$

$$\kappa_L = \frac{30000}{29} \cdot \frac{1}{R^2}; \quad (47)$$

$$\phi(x) = \frac{\exp(-x^2)}{\sqrt{\pi}}. \quad (48)$$

Note that, in Sections 9 and 15 of Avrett & Loeser (1984) where they have $\sigma = 0$ and a value of κ_A which is twice that given in equation (46), these conditions are identical to cases 2 and 4 because both use $J_{x,c}$ from case 1 in the background source term. That is, since here $\kappa_A = \sigma$, and $S_A = 1.0$ (Table 1) the background monochromatic source term, S_B , can be written as

$$S_B = \frac{\sigma J_{x,c}}{\sigma + \kappa_A} + \frac{\kappa_A S_A}{\sigma + \kappa_A} = \frac{1}{2} (J_{x,c} + 1.0) \quad (49)$$

which is equal to that given in (AL-18) with $\alpha = 1/2$.

4.1.3 Specifications of atmospheric parameters

The spherical atmosphere has outer and inner boundaries at R_1 and R_N stellar radii, respectively. The geometric length being measured in terms of the stellar radius. The inner and outer boundaries are at 1 and 30 stellar radii, *i.e.* $R_1 = 30$ and $R_N = 1$.

The non-relativistic velocity field adopted in case 4 is given by (AL-101), namely,

$$V(R) = \frac{6}{\pi} \left[\tan^{-1} \left(\frac{2R - 31}{29} \right) + \frac{\pi}{4} \right]. \quad (50)$$

The velocity is in units of the Doppler width and is expressed, as usual, as

$$V_{Dopp} = c \frac{\Delta \nu_{Dopp}}{\nu_0}. \quad (51)$$

4.1.4 Specification of depth and frequency grids

For the comparison we use $ndep = 50$ depth-points. We also use three interpolation points between the last and penultimate depth-points for all core rays and at the tangent, as described previously. The number of frequency points, nq , is 10 for the static atmosphere and 25 for the moving atmosphere. It is assumed that $\tau = 0$ at the upper boundary and there is no incoming radiation. The depth point spacing for these cases was chosen as follows:

1. A constant $\Delta \log \tau$ scale with $ndep - 1$ points, is constructed. The maximum optical depth at the penultimate depth-point is $\tau = 1.0 \times 10^{-3}$.
2. An additional point is added at the outer boundary at $\tau = 0$.
3. To compare our results with the published tabulations, we have made cubic spline interpolations of the tabulated quantities from our atmospheric grid.

In the case of the line transfer problem the optical depth scale is the frequency-independent opacity $\bar{\tau} = - \int \kappa_L dR$. The total monochromatic optical depth is then (AL-64)

$$\tau_x = \bar{\tau} \frac{\exp(-x^2)}{\sqrt{\pi}} - \int (\kappa_A + \sigma) dR.$$

4.1.5 Method of solution

Since these cases are idealized, the following test cases were computed with a separate code which uses the same spherical modifications as are present in S-MULTI but not the Scharmer operator. The solution to each radiative transfer problem was made using an accelerated lambda iteration scheme with Ng acceleration.

4.2 Results of comparison

In the following tables the results from previous investigations are those of Mihalas, Kunasz & Hummer (1975), Avrett & Loeser (1984) and Rogers (1984). The results of Mihalas *et al.* (1975) are results that have been reported in Avrett & Loeser (1984) and Rogers (1984). Avrett & Loeser (1984) also report some results from Rogers that do not appear in Rogers (1984).

The four different investigations have used different boundary conditions at the inner boundary. Mihalas *et al.* (1975) and Rogers (1984) use a transparent core while Avrett & Loeser (1984) and ourselves have used an opaque core. In the line transfer examples the adopted value of collisional de-excitation parameter, ϵ , is such that the source functions are nearly thermalized so that the different boundary conditions only lead to small differences in the solutions near the core boundary. The differences due to the different boundary conditions are discussed below.

4.2.1 Test case 1

Table 2 gives a comparison of the mean intensity calculated here and in the above references. Three cases are given for the present scheme (a) opaque core with geometric weights, $C(mu, k + 1)$, (b) transparent core with geometric weights and (c) transparent core with exact weights computed for the opacity distribution in this example.

It can be seen that overall the results for cases with the same core boundary condition agree to within 0.7 per cent at the core and 1.6 per cent at $R = 30R_*$. This close agreement verifies that the algorithms used by the different investigators are suitable for solving the monochromatic problem in spherical geometry. The level of agreement between the different techniques is of the same order but slightly larger than that from using different depth-scales with the same technique. Comparison of the results for (a) and (b) show that the influence of the boundary condition is noticeable out to $2R_*$ but not farther out. Cases (b) and (c) which compare with the results of Mihalas *et al.* (1975) and Rogers show that our results are very close to those of Rogers. We also compared our results to those found using a depth-scale that had been constructed as described previously but with an even spatial grid and found the maximum difference to be < 0.5 per cent. Most of the differences in the outer layers will be due to the different depth-scales and subtle differences between the techniques.

Table 2: Mean monochromatic intensity $J_{x,c}$ at selected radial distances R/R_* , cf. Avrett & Loeser (1984), table 1. The three results from this work are for (a) opaque core and geometric weights (b) transparent core and geometric weights and (c) transparent core and exact weights (see text for details).

Radius (R_*)	$J_{x,c}$ [1]	$J_{x,c}$ [2]	$J_{x,c}$ [3]	$J_{x,c}$ [4]a	$J_{x,c}$ [4]b	$J_{x,c}$ [4]c
30.0	0.0636	0.0638	0.0642	0.0632	0.0632	0.0638
29.6	0.0671	0.0674	0.0676	0.0669	0.0669	0.0674
29.0	0.0716	0.0716	0.0721	0.0714	0.0714	0.0719
28.0	0.0784	0.0785	0.0791	0.0782	0.0782	0.0788
26.0	0.0920	0.0921	0.0928	0.0918	0.0918	0.0925
24.0	0.106	0.107	0.108	0.106	0.106	0.107
20.0	0.141	0.140	0.142	0.140	0.140	0.141
16.0	0.182	0.187	0.190	0.186	0.186	0.188
12.0	0.260	0.255	0.261	0.255	0.255	0.258
9.0	0.345	0.336	0.340	0.336	0.336	0.339
6.0	0.493	0.468	0.476	0.468	0.468	0.473
4.0	0.638	0.615	0.627	0.616	0.616	0.620
2.0	0.864	0.849	0.859	0.850	0.849	0.853
1.0	0.964	0.961	0.986	0.982	0.958	0.959

[1] Mihalas *et al.* (1975).

[2] Rogers as reported in Avrett & Loeser (1984).

[3] Avrett & Loeser (1984).

[4] Harper, this paper.

Table 3: Line source function, S_L , at selected values of radial distance, R/R_* , for a static atmosphere with a frequency-independent continuum source function, cf. Rogers (1984). The number of significant figures given for the radius corresponds to those given in Rogers (1984) table 1.

Radius (R_*)	S_L [1]	S_L [4]	S_L [5]
30.00	0.04249	0.04228	0.04241
29.867	0.04963	0.04932	0.04965
28.365	0.09699	0.09650	0.09674
24.470	0.1925	0.1911	0.1922
18.456	0.3336	0.3301	0.3331
12.723	0.4849	0.4782	0.4820
8.93	0.6050	0.5949	0.5962
4.33	0.7941	0.7817	0.7843
2.0191	0.9321	0.9228	0.9264
1.000	0.9826	0.9775	0.9936

[1] Mihalas *et al.* (1975).

[4] Harper, this paper.

[5] Rogers (1984).

Case (c), with weights that correspond to this particular example, gave best agreement with the results of Rogers in the outer layers but made no noticeable improvement deeper in.

4.2.2 Test case 2

Tables 3 and 4 show the results for the line transfer with a frequency-independent background source function. The results of Mihalas *et al.* (1975) actually refer to a calculation in an expanding atmosphere with $V_{max} = 0.1V_{micro}$ but the results should be the same as in the static atmosphere to within about three significant figures (Avrett & Loeser 1984). In Table 3 we have used a transparent core in order to make a more detailed comparison.

The normalized line profile is very similar to that of Rogers (1984) but greater than that of Avrett & Loeser by less than 3 per cent. The line source function is in very good agreement with those in Mihalas *et al.* (1975) and Rogers (1984) except at the deepest point. Our solution is, on the whole, systematically lower by 0.5 per cent. The internal errors in Rogers' (1984) results are estimated to be a few tenths of a percent. We ran the same case with the opaque core and found similar good agreement, but this time closer agreement at the core boundary. With an opaque core the

Table 4: Normalized flux profile, F_x , in the static case with a frequency-independent continuum source function, cf. Avrett & Loeser (1984) table 3 and Rogers (1984) table 2.

x	F_x [5]	F_x [3]	F_x [4]
0.0	0.4009	0.392	0.4037
0.4	0.4237	0.414	0.4267
0.8	0.5078	0.496	0.5112
1.2	0.7024	0.685	0.7058
1.6	1.0210	0.992	1.0231
2.0	1.1835	1.154	1.1835
2.4	1.0745	1.064	1.0743
2.8	1.0113	1.010	1.0112
3.2	1.0009	1.001	1.0010
3.6	1.0000	1.000	1.0000

[3] Avrett & Loeser (1984).

[4] Harper, this paper.

[5] Rogers (1984).

Table 5: Line source function, S_L , at selected values of radial distance, R/R_* , and line centre optical depth, $\bar{\tau}$, for the static atmosphere with a frequency-dependent continuum source function, cf. Rogers (1984) table 3.

Radius (R_*)	$\bar{\tau}$	S_L [5]	S_L [4]
30.0	0.0	0.04562	0.04545
29.9133	1.00000×10^{-1}	0.05110	0.05075
29.7207	3.24065×10^{-1}	0.05983	0.05933
29.1133	1.05018	0.08136	0.08106
27.3051	3.40328	0.1352	0.1346
22.7301	$1.10289 \times 10^{+1}$	0.2592	0.2574
14.7313	$3.57408 \times 10^{+1}$	0.5031	0.4972
6.88250	$1.15823 \times 10^{+2}$	0.8131	0.8105
3.01571	$3.08549 \times 10^{+2}$	0.9705	0.9643
1.0	$1.00000 \times 10^{+3}$	1.001	0.9982

[5] Rogers (1984).

[4] Harper, this paper.

source functions were about 0.5 per cent less than with a transparent core. The calculated source functions from Mihalas *et al.* (1975) and Rogers agree to within 1.5 per cent, while these two are reported to be within 5 per cent of those calculated by Avrett & Loeser (1984). With either boundary condition we are in significantly closer agreement with Mihalas *et al.* (1975) and Rogers (1984) than we are with Avrett & Loeser (1984). We also compared our result to Table 1B of Rogers (1984) and again found the same level of agreement.

4.2.3 Test case 3

The results for the line transfer with a frequency-dependent background source function are given in Tables 5 and 6. We use the transparent core as a lower boundary condition.

Our line source function agrees closely with the results of Rogers, with a maximum difference of 1.2 per cent. The noticeable difference noted in case 2 at the lower boundary does not appear in this case. Our normalized line profile also agrees well (to within 0.7percent) with that of Rogers. The normalized line profile calculated by Avrett & Loeser (1984) is lower and differs from ours by up to 7 per cent. It would seem from the previous two cases that there is a small systematic difference between the results of Avrett & Loeser (1984) and the other calculations.

Table 6: Normalized flux profile, F_x , for the static atmosphere with a frequency-dependent continuum source function, cf. Rogers (1984) table 4.

x	F_x [3]	F_x [4]	F_x [5]
0.0	0.417	0.4342	0.4315
0.4	0.441	0.4594	0.4567
0.8	0.530	0.5522	0.5493
1.2	0.736	0.7702	0.7676
1.6	1.073	1.1388	1.1385
2.0	1.232	1.3234	1.3262
2.4	1.091	1.1360	1.1374
2.8	1.014	1.0214	1.0214
3.2	1.001	1.0019	1.0018
3.6	1.000	1.0000	1.0000

[3] Avrett & Loeser (1984).

[4] Harper, this paper.

[5] Rogers (1984).

Table 7: Line source function, S_L , at selected values of radial distance, R/R_* , and line centre optical depth, $\bar{\tau}$, for an expanding atmosphere with $V_{max} = 3$, from Mihalas *et al.* (1975). (cf. Avrett & Loeser (1984) table 6). The frequency grid is that of Avrett & Loeser (1984) in their table 7.

R (R_*)	$\bar{\tau}$	S_L [1]	S_L [4]
30.00	0.0	0.03652	0.03640
29.99	9.595×10^{-3}	0.03713	0.03717
29.87	1.541×10^{-1}	0.04264	0.04245
29.29	8.343×10^{-1}	0.05989	0.05980
28.37	1.988	0.08194	0.08150
26.87	4.013	0.1126	0.1119
24.47	7.794	0.1573	0.1556
21.53	$1.357 \times 10^{+1}$	0.2114	0.2085
18.46	$2.158 \times 10^{+1}$	0.2737	0.2710
15.86	$3.078 \times 10^{+1}$	0.3362	0.3287
12.72	$4.697 \times 10^{+1}$	0.4293	0.4185
8.93	$8.215 \times 10^{+1}$	0.5730	0.5572
4.33	$2.151 \times 10^{+2}$	0.7903	0.7783
2.02	$5.085 \times 10^{+2}$	0.9320	0.9248
1.00	$1.046 \times 10^{+3}$	0.9827	0.9916

1 Mihalas, D., Kunasz, P. B., Hummer, D., (1975).

4 Harper, G. M., this paper.

4.2.4 Test case 4

The results for the line transfer in an expanding atmosphere with a frequency-independent continuum source function are given in Tables 7 and 8 and Fig. 3.

We have used an opaque boundary condition and our line source function agrees with that of Mihalas *et al.* (1975) to within 3percent with a similar systematic behaviour as is seen in case 2. The source functions of Avrett & Loeser (1984) are reported to agree with Mihalas *et al.* (1975) to within about 8 per cent. Our normalized line profile is up to 10 per cent greater than that of Avrett & Loeser (1984) (Table 8), however the profile of Mihalas *et al.* (1975) (Fig. 8 of that paper) is in better agreement with our results.

Table 8: Normalized flux profile, F_x . for an expanding atmosphere with $V_{max} = 3$. (cf. Avrett & Loeser (1984) table 7).

$ x $	$F_x(\text{red half})$ [3]	$F_x(\text{blue half})$ [3]	$F_x(\text{red half})$ [4]	$F_x(\text{blue half})$ [4]
0.0	0.91	0.91	0.99	0.99
0.4	1.08	0.74	1.18	0.81
0.8	1.23	0.59	1.34	0.64
1.2	1.36	0.47	1.47	0.51
1.6	1.43	0.39	1.53	0.43
2.0	1.43	0.35	1.53	0.37
2.4	1.37	0.34	1.46	0.37
2.8	1.27	0.37	1.34	0.39
3.2	1.17	0.43	1.22	0.45
3.6	1.08	0.54	1.11	0.56
4.0	1.02	0.72	1.04	0.74
4.5	1.01	0.93	1.01	0.93
5.5	1.00	1.00	1.00	1.00

[3] Avrett, E. H, Loeser, R., (1984).

[4] Harper, G. M., this Paper.

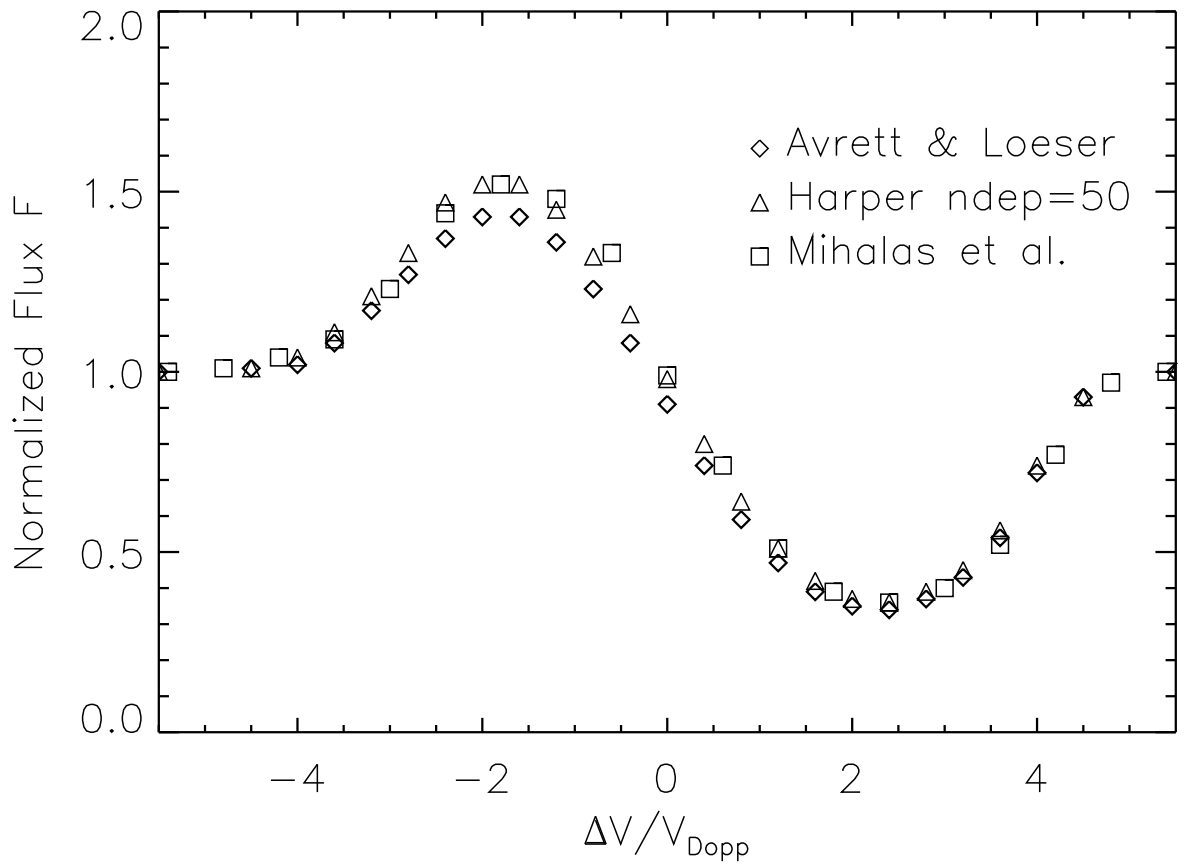


Figure 3: Line profile for the expanding atmosphere with a frequency-independent continuum source function (cf. Avrett & Loeser 1984, fig. 10). These profiles are calculated from three independent schemes, Mihalas *et al.* (1975), Avrett & Loeser (1984) and this paper.

4.2.5 Summary of test calculations

The different test cases show that the adopted algorithms in S-MULTI produce results in good agreement with those from three independent investigations. Our line source functions are very close to those of Rogers (1984), and are within 3 per cent of those of Mihalas *et al.* (1975) in the important moving atmosphere example. We find that our results are significantly closer to those of Rogers and Mihalas *et al.* (1984) than to those of Avrett & Loeser (1984).

These comparisons show that in simple test cases (see also later) the calculations of the radiation fields and line profiles should be accurate to within *3percent* for the static atmosphere and 5 per cent for the moving atmosphere. The comparisons give useful lower bounds to the uncertainties in calculations of atmospheres which are more extended than considered here, and have higher velocity gradients. The differences due to the choice of depth-scale are small for the static atmospheres, and are ~ 2 per cent for the moving atmospheres, when the maximum optical depth is 10^3 and the atmospheric model has 50 depth-points.

4.3 Further exploratory calculations

We examine the moving atmosphere calculation described above and show the sensitivity of the calculated line profile to the following computational grids:

1. the number of depth points (*ndep*);
2. the number of core rays (*ncore*);
3. the number of interpolation points (*nintep*).

We vary one grid at a time, keeping the other values as described in the text. For comparison, we take the *most accurate* results as those that have been computed with a fine grid, namely $ndep = 200$, $ncore = 20$, $nintep = 20$, $nq = 50$. This provides a reference profile. Fig. 4 shows the information shown in Fig. 3 together with the fine grid described here.

4.3.1 Depth points

The static line centre optical depth for the expanding atmosphere example covered over six orders of magnitude. With a constant $\Delta \log \tau$ scale and $ndep = 50$ this gives $\Delta \log \tau \sim 0.12$. This is smaller than is often considered in stellar studies, and typically a value < 0.3 is desirable for the cases that we consider. In the expanding atmosphere, however, the spacing is more critical because of the projected Doppler shifts of opacity between grid-points. A grid of $ndep = 25$ approximately corresponds to $\Delta \log \tau \sim 0.3$ for the line and represents the minimum desirable number of depth-points. Fig. 5 shows three profiles which correspond to $ndep = 25, 50, 100$ and the reference profile.

The profile that corresponds to $ndep = 25$ shows significant departures from the fine grid example and demonstrates that this is the minimum number of required depth-points.

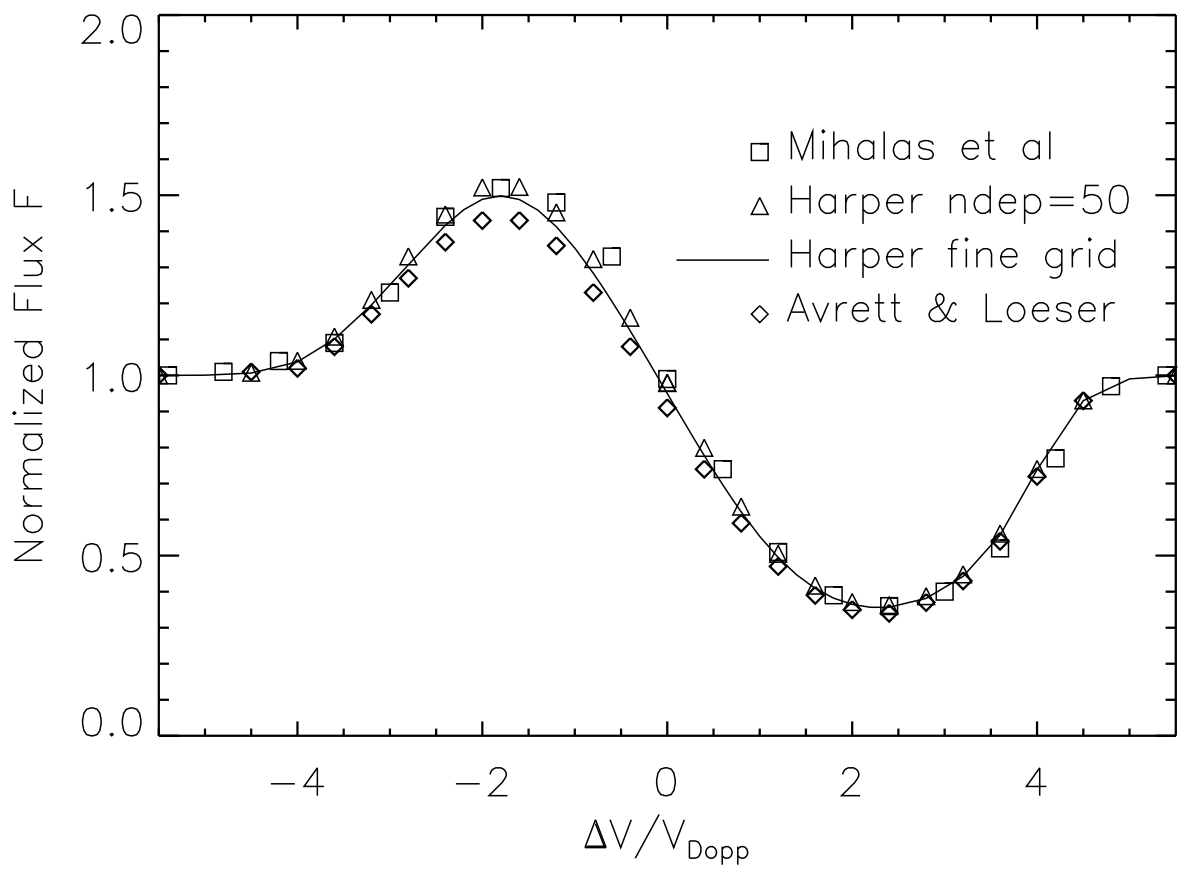


Figure 4: Further comparison of the line flux profiles. The reference profile (fine grid) is shown together with profile calculated with $ndep = 50$, Mihalas *et al.* (1975) and Avrett & Loeser (1984).

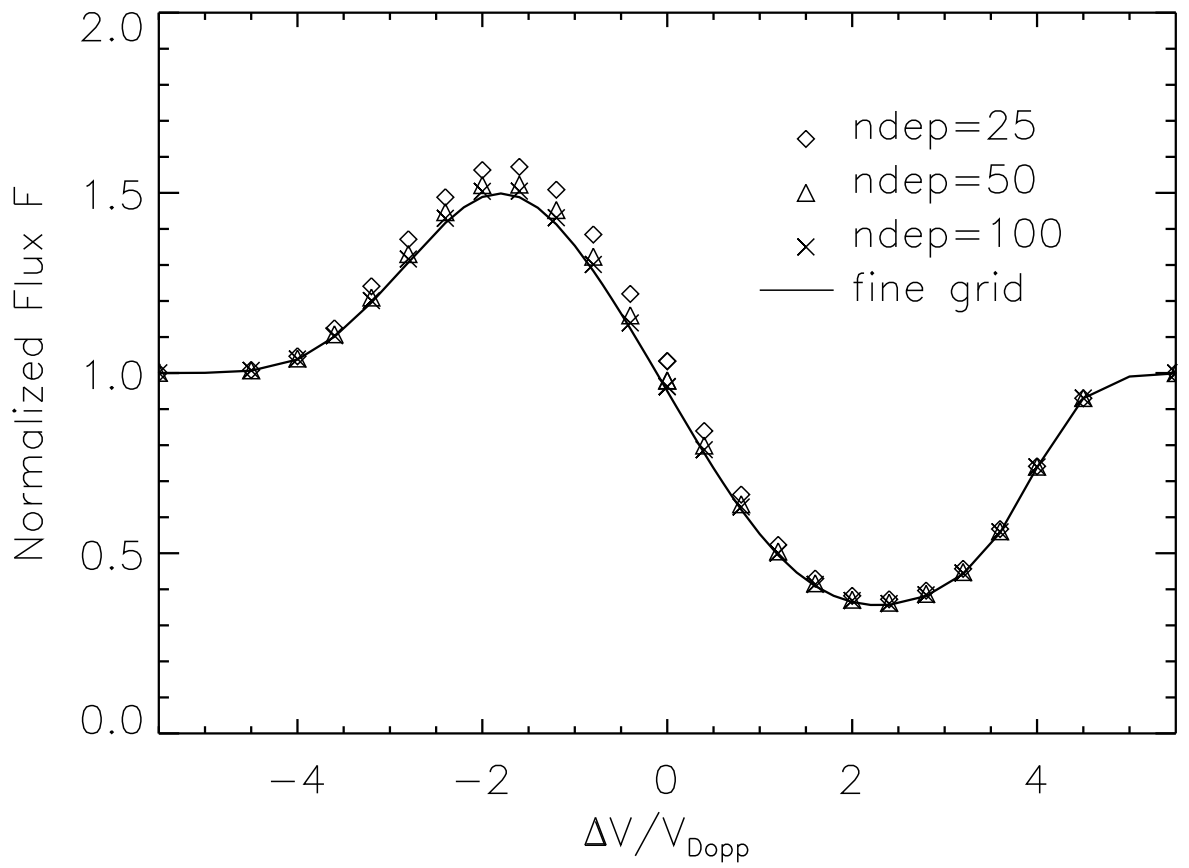


Figure 5: Sensitivity of the line flux profile to the number of depth points. The cases where $ndep = 25, 50$ and 100 and the fine grid are shown.

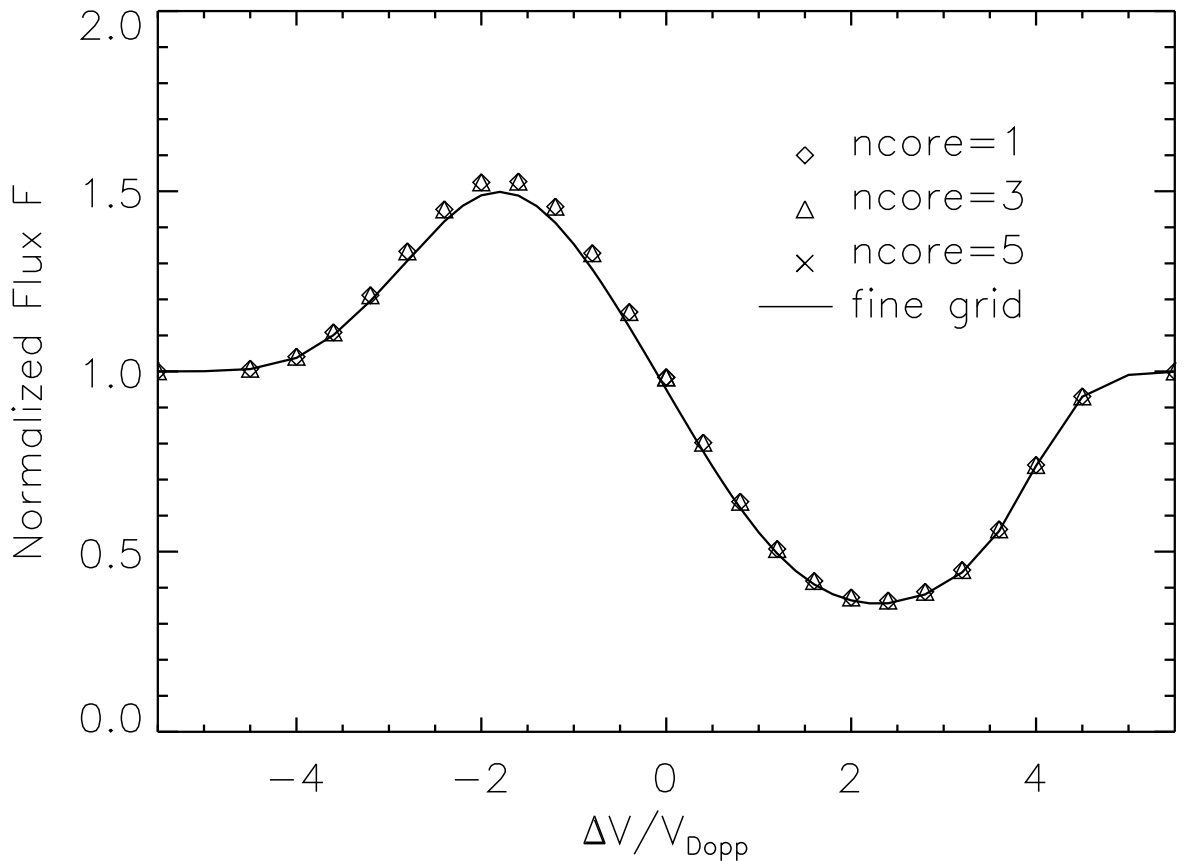


Figure 6: Sensitivity of the line flux profile to the number of core rays.

4.3.2 Core rays

Fig. 6 shows the sensitivity of the line profile in this particular example. The point at which the line optical depth is unity is in the outer atmosphere and this is reflected in the insensitivity of the line profile to the number of rays intersecting the core in this example. In stellar atmospheres near the photosphere, the optical depths of radiative transitions can change rapidly with distance. For a transition with an optical depth of unity near the stellar surface a single core ray would lead to an insufficiently accurate intensity quadrature. A rough *rule of thumb* for the number of core rays would be $> 2n - 1$ where n is the number of rays used in plane-parallel calculations with Gaussian quadrature.

4.3.3 Interpolation points

The moving atmosphere example (case 4) considered here, is in the low-velocity regime, with $V_{\max}/V_{\text{micro}} = 3$. Along the normal of the atmosphere, with the adopted number of depth points

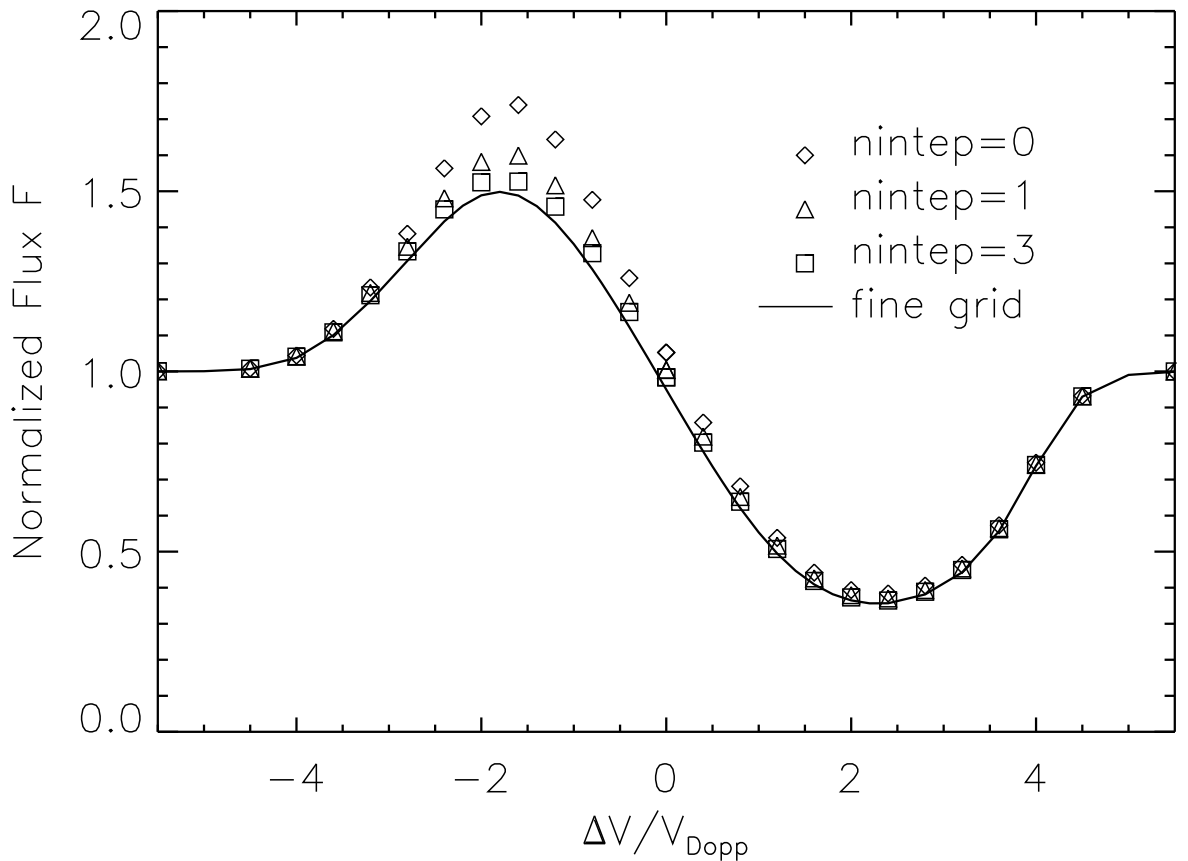


Figure 7: Sensitivity of the line flux profile to the number of interpolation points between the last and penultimate atmospheric grid points of each ray. Note that the absence of any interpolation points leads to a profile that is significantly different from a more complete calculation.

there are sufficient points to keep the changes in wind velocity within $0.5V_{micro}$ between depth points. The coupling of the frequency with angle, however, means that the tangent ray needs to be treated with care. Fig. 7 shows the influence of the number of interpolation points added at the tangent on the normalized line profile.

The effect is striking; with no interpolation points the profile is inaccurate and becomes sensitive to the location of the depth points. This demonstrates the utility of this technique and its use in other codes described in the literature. We find that $nintep = 3$ gives agreement to within 2 per cent with the reference profile. Because the angles of the rays are the same for the profiles corresponding to $nintep = 0, 1, 3$ the difference in the profiles reflects the effects of the opacity sampling at the tangent on the formal solution of each ray. This effect is not dependent on the presence of a velocity gradient, even a constant velocity field will lead to this effect since it is the projection of velocity along the line of sight that is important. For more extended atmospheres, more depth points and more interpolation points will be needed for wind flow with a $V_{max} = 3$.

5 CONCLUSIONS

We have described modifications to the code MULTI which generalize it to spherical symmetry. The code is suitable for atmospheres where the wind velocity is up to several times the turbulent velocity, *i.e.* in the regime where the Sobolev approximation is not valid. Comparisons with the results from three independent investigations show that the geometric scheme is accurate and reliable provided that sufficient depth-points are used. It is found that the treatment of the velocity field near the tangent is the single most important aspect of the moving atmosphere problem. Limits to the accuracy of the results for this scheme are given. An approximate global operator is presented which has been demonstrated to be useful in stellar atmosphere calculations. The subroutines necessary to include spherical geometry in MULTI and additional details are available from the author.

Acknowledgments

This research was funded by the SERC grants GR/G 50308 and GR/G 06107, and the computations were made on the Department of Physics (Theoretical Physics) SUN workstation cluster at Oxford University. I especially thank Dr Carole Jordan for her continued support and encouragement and also for helping to improve the clarity of this manuscript. I also thank Dr M. Carlsson for valuable comments on the manuscript, Drs D. Sasselov, H. Uitenbroek and P. Judge for discussions on this work and Dr P. Bennett for helpful suggestions. I thank the Solar and Stellar Physics Division of the Harvard Smithsonian Center for Astrophysics for making funds available for collaborative work. This work is dedicated to the memory of Rev. A. Bamford.

References

- Anderson L. S., 1992, in Giampapa M., Bookbinder J. A., eds, Cool stars, stellar systems, and the sun. 7th Cambridge Workshop, ASP Conf. Ser. 26, p. 509
- Auer, L. H., 1987, in Kalkofen W., ed, Numerical radiative transfer. Cambridge Univ. Press, Cambridge p. 101
- Auer L. H., Heasley J. N., Milkey R. W., 1972, Kitt Peak Nat. Obs. Contrib. No. 555
- Avrett E. H., Loeser R., 1984, in Kalkofen W., ed, Methods in radiative transfer. Cambridge Univ. Press, Cambridge p. 341
- Avrett E. H., Loeser R., 1992, in Giampapa M., Bookbinder J. A., eds, Cool stars, stellar systems, and the sun. 7th Cambridge Workshop, ASP Conf. Ser. 26, p. 489
- Ayres T. R., 1979, ApJ, 228, 509
- Ayres T. R., Linsky J. L., 1975, ApJ, 200, 660
- Baade R., 1990, in Evolution in astrophysics, ESA SP-310, p.65
- Baade R., 1992, in Jeffery C. S., Griffin R. E. M., eds, Stellar chromospheres, coronae and winds: CCP7 Workshop. IOA, Cambridge, p. 49
- Baschek B., Scholz M., Wehrse R., 1991, A&A, 246, 374
- Basri G. S., Linsky J. L., Eriksson K., 1981, ApJ, 251, 162
- Cannon C. J., 1985, The transfer of spectral line radiation, Cambridge Univ. Press, Cambridge, p. 148
- Carlsson M., 1986, A computer program for solving multi-level non-LTE radiative transfer problems in moving or static atmospheres, Uppsala Astronomical Observatory, Report No. 33 (MULTI)
- Carlsson M., 1991, in Crivellari L., Hubeny I., Hummer D. G., eds, Stellar Atmospheres: Beyond Classical Models. NATO ASI Series Vol. 341, Kluwer Academic Publishers, p. 34
- Carlsson M., 1992, in Giampapa M., Bookbinder J. A., eds, Cool stars, stellar systems, and the sun. 7th Cambridge Workshop, ASP Conf. Ser. 26, p. 499
- Drake S. A., 1985, in Beckman J. E., Crivellari L., eds, Progress in Stellar Spectral Line Formation Theory. D. Reidel Publishing Company, p. 351
- Drake S. A., Brown A., Linsky J. L., 1984, ApJ, 284, 774
- Glasse A. C. H., 1989a, in Lecture Notes in Physics, Springer-Verlag, Berlin, No. 331, p. 318
- Glasse A. C. H., 1989b, in CCP7 Newsletter on Analysis of Astrophysical Spectra, No. 13, Daresbury Laboratory, p. 38
- Gray D. F., 1992, The observation and analysis of stellar photospheres, Cambridge Univ. Press, p. 431
- Gustafsson B., 1973, Uppsala Astron. Obs. Ann., Vol. 5, No. 6
- Harper G. M., 1992, MNRAS, 256, 37
- Harper G. M., 1994, Cool stars, stellar systems, and the sun. 8th Cambridge Workshop, A.S.P. Conf. Series, in Press
- Hartmann L., Avrett E. H., 1984, ApJ, 284, 238
- Hartmann L., Dupree A. K., Raymond J. C., 1980, ApJ, 236, L143
- Hartmann L., Dupree A. K., Raymond J. C., 1980, ApJ, 246, 193
- Hummer D. G., Voels S. A., 1988, A&A, 192, 279
- Islaker H., Nussbaumer H., Vogel M., 1989, A&A, 219, 271
- Jeffery C. S., 1992, in Collaborative Computational Project, No. 7, Newsletter No. 17, Daresbury

- Laboratory, p.43
- Jordan C., Linsky J. L., 1987, in Kondo Y., ed, Exploring the Universe with the IUE Satellite. D. Reidel Publishing Company, p. 259
- Judge P. G., 1990, ApJ, 348, 279
- Kalkofen W., 1984, Methods in radiative transfer, Cambridge Univ. Press, Cambridge
- Kuiper G. P., Struve O., Strömgren B., 1937, ApJ, 86, 570
- Linsky J. L., 1985, in Beckman J. E., Crivellari L., eds, Progress in Stellar Spectral Line Formation Theory. D. Reidel Publishing Company, p. 1
- Luttermoser D. G., 1992, in Giampapa M., Bookbinder J. A., eds, Cool stars, stellar systems, and the sun. 7th Cambridge Workshop, ASP Conf. Ser. 26, p. 506
- Martin P. G., Rogers C., Rybicki G. B., 1984, ApJ, 284, 317
- Menzel D. H., 1931, Publications of the Lick Observatory, Vol. XVII, p. 242
- Menzel D. H., circa 1936, Harvard College Obs. Circular 417, 1
- Mihalas D., 1978, Stellar Atmospheres, W. H. Freeman and Company - San Francisco., p. 451
- Mihalas D., Kunasz P. B., Hummer D. G., 1975, ApJ, 202, 465
- Ng K-C, 1974, J. Chem. Phys., Vol. 61, No. 7, 2680
- Nordlund Å., 1982, A&A, 107, 1
- Nordlund Å., 1984, in Kalkofen W., ed, Methods in radiative transfer. Cambridge Univ. Press, Cambridge p. 211
- Olson G. L., Auer L. H., Bulcher J. R., 1986, J. Quant. Spectrosc. Radiat. Transfer, 35, 431
- Paresce F., 1984, AJ, 89, 1022
- Puls J., Herrero A., 1988, A&A, 204, 219
- Reimers D., 1982, A&A, 107, 292
- Reimers D., 1987, in Appenzeller I., Jordan C., eds, IAU Symposium No. 122, Circumstellar Matter, p. 307
- Rogers B., Glassgold A. E., 1991, ApJ, 382, 606
- Rogers C., 1981, Ph. D. Thesis, University of Toronto
- Rogers C., 1984, ApJ, 286, 659
- Rogers C., Martin P. G., 1984, ApJ, 284, 327
- Rybicki G. B., 1984, in Kalkofen W., ed, Methods in radiative transfer. Cambridge Univ. Press, Cambridge p. 21
- Rybicki G. B., Hummer D. G., 1991, A&A, 245, 171
- Scharmer G. B., 1981, ApJ, 249, 720
- Scharmer G. B., 1984, in Kalkofen W., ed, Methods in radiative transfer. Cambridge Univ. Press, Cambridge p. 173
- Scharmer G. B., Carlsson M., 1985a, J. Comp. Phys., Vol. 59, No. 1, 56
- Scharmer G. B., Carlsson M., 1985b, in Beckman J. E., Crivellari L., eds, Progress in Stellar Spectral Line Formation Theory. D. Reidel Publishing Company, p. 189
- Schmidt M., Gesicki K., 1992, in Jeffery C. S., Griffin, R. E. M., eds, Stellar chromospheres, coronae and winds: CCP7 Workshop. IOA, Cambridge, p. 88
- Schröder K.-P., Reimers D., Carpenter K. G., Brown A., 1988, A&A, 202, 136
- Sykes J. B., 1951, MNRAS, 111, 377
- Troland T. H., Heiles, C., 1986, ApJ, 301, 339
- Uitenbroek H., 1989a, A&A, 213, 360

Uitenbroek H., 1989b, A&A, 216, 310
Uitenbroek H., Bruls J. H. M. J., 1992, A&A, 265, 268
Vernazza J. E., Avrett E. H., Loeser R., 1981, ApJS, 45, 635
Vogel M., 1991, A&A, 249, 173

Appendix A Optical depth scaling factors

Here we consider the scaling factors for the rays when $mu \neq 1$. In this example the opacity per hydrogen atom is constant, so the optical depth increment between two depth-points can be written in terms of the hydrogen column density increment, $\Delta hcol$,

$$\Delta\tau(mu, k) = \kappa \cdot \Delta hcol(mu, k). \quad (A1)$$

Consider $\Delta hcol$, along a ray which is at an angle of θ with the normal at depth-point $k + 1$. Defining Z as the geometric path along the ray from $k + 1$ to k , such that $Z(k + 1) = 0$ and $Z(k) = Zk$. This path is between shells whose radii correspond to depth points k and $k + 1$ (where $R(k) > R(k + 1)$). This distance, Zk , is determined by the overall spatial distribution of depth-points. This increment is defined as

$$\Delta hcol(mu, k) = \int_0^{Zk} N_H(Z) dZ \quad (A2)$$

where Zk is the path-length between the shells for the angle θ . We assume that the hydrogen density has the form

$$N_H(R) = N_H(k + 1) \left(\frac{R(k + 1)}{R} \right)^2. \quad (A3)$$

Using the relation for a general plane triangle to write the radial distance, R , in terms of Z , and completing the square we obtain

$$\begin{aligned} R^2 &= R^2(k + 1) + Z^2 - 2 \cdot R(k + 1) \cdot Z \cdot \cos(\pi - \theta) \\ &= [R(k + 1) \cos(\theta) + Z]^2 + R^2(k + 1) [1 - \cos^2(\theta)]. \end{aligned} \quad (A4)$$

The increment in the column density becomes

$$\Delta hcol(mu, k) = \int_0^{Zk} \frac{N_H(k + 1) R^2(k + 1)}{[R(k + 1) \cos \theta + Z]^2 + R^2(k + 1) [1 - \cos^2 \theta]} dZ. \quad (A5)$$

Using the trigonometric substitution

$$\int \frac{1}{x^2 + a^2} dx = \frac{1}{a} \tan^{-1} \left(\frac{x}{a} \right) + c \quad (A6)$$

when $a \neq 0$, ($\theta \neq 0$), and letting $x = R(k + 1) \cos \theta + z$ and $a = R(k + 1) \sqrt{1 - \cos^2 \theta} = R(k + 1) \sin \theta$, we obtain

$$\Delta hcol(mu, k) = \frac{N_H(k + 1) R(k + 1)}{\sin \theta} \left[\tan^{-1} \left\{ \frac{R(k + 1) \cos \theta + Z}{R(k + 1) \sin \theta} \right\} \right]_0^{Zk}. \quad (A7)$$

Now, dividing the angle into two parts (when $\theta \neq 0$), and noting relation (A4),

$$\Delta hcol(mu, k) = \frac{N_H(k + 1) R(k + 1)}{\sin \theta} \left[\tan^{-1} \{ \cot \theta \} + \sin^{-1} \left\{ \frac{Z \sin \theta}{R} \right\} \right]_0^{Zk}. \quad (A8)$$

Then, taking the limits

$$\Delta h_{col}(mu, k) = \frac{N_H(k+1)R(k+1)}{\sin \theta} \left[\sin^{-1} \left\{ \frac{Zk \sin \theta}{R(k)} \right\} \right]. \quad (\text{A9})$$

The corresponding increment along the normal (when $\cos \theta = 1$) is given by

$$\Delta h_{col}(mu, k) = N_H(k+1)R(k+1) \left[\frac{R(k) - R(k+1)}{R(k)} \right]. \quad (\text{A10})$$

The ratio of the increment along the ray with angle θ to the normal $\theta = 0$ correspond to the matrix elements in $C(mu, k+1)$. Thus

$$C(mu, k+1) = \frac{1}{\sin \theta} \left[\sin^{-1} \left\{ \frac{Zk \sin \theta}{R(k)} \right\} \right] \cdot \left[\frac{R(k)}{R(k) - R(k+1)} \right]. \quad (\text{A11})$$

As $\theta \rightarrow 0$, then $C(mu, k+1) \rightarrow 1$ for all depth points, in this case $Zk = R(k) - R(k+1)$, $\sin \epsilon \rightarrow \epsilon$, $\cos \epsilon \rightarrow 1$ and $\sin^{-1} \epsilon \rightarrow \epsilon + (\epsilon^3/6)$, *i.e.*

$$C(mu \rightarrow 1, k+1) \rightarrow \frac{1}{\theta} \left[\left\{ \frac{\theta (R(k) - R(k+1))}{R(k)} \right\} \right] \cdot \left[\frac{R(k)}{R(k) - R(k+1)} \right] \rightarrow 1, \quad (\text{A12})$$

as required. At the outer boundary, where $k+1 = 1$, the correction for overlying opacity in the formal solution uses $C(mu, 1)$ (see text). This corresponds to $R(0) \rightarrow \infty$, while $R(1)$ remains finite. In this case, for any angle, we obtain

$$C(mu, 1) \rightarrow \frac{1}{\sin \theta} \left[\sin^{-1} \left\{ \frac{\sin \theta R(k)}{R(k)} \right\} \right] \cdot \left[\frac{R(k)}{R(k)} \right] \rightarrow \frac{\theta}{\sin \theta}, \quad (\text{A13})$$

which tends to unity for $\theta \rightarrow 0$ and has a *limiting* value of $\pi/2$, as opposed to the case of plane-parallel geometry, where this term tends to infinity.

The difference between the geometrical weights and those above can be estimated as follows from equation (A11). The ratio, R_w , of these inverse-square to geometrical weights is

$$R_w = \frac{1}{x} \sin^{-1} x \quad \text{where} \quad x = \frac{Zk \sin \theta}{R(k)}$$

Because $0 < x \leq 1/2$, then $R_w \geq 1.0472$. Thus the geometrical weights are less than those from this specific opacity distribution. In most cases $x \ll 0.5$ so $R_w \sim (x + x^3/6)/x \sim 1 + x^2/6$.